COMPARATIVE STUDY AND IMPROVEMENTS ON MESH-FREE LAGRANGIAN COMPUTATIONAL FLUID DYNAMICS

A Thesis

by

FARID PUTRA BAKTI

Submitted to the Office of Graduate and Professional Studies of
Texas A&M University
in partial fulfillment of the requirements for the degree of

MASTER OF SCIENCE

Chair of Committee,	Moo-Hyun Kim
Committee Members,	Hamn-Ching Chen
	Achim Stössel
Head of Department,	Robin Autenrieth

August 2015

Major Subject: Ocean Engineering

ABSTRACT

Mesh-free Lagrangian Computational Fluid Dynamics is a numerical scheme where the computational points are represented by freely-moving finite particles that have a constant mass. Smoothed Particle Hydrodynamics (SPH) and Moving Particle Semi Implicit (MPS) method are two prominent methods that utilized the above-mentioned framework. Both methods principal advantages are best exploited when simulating large deformation and fragmentation of free surface. Although sharing the same framework, both methods have several differences, especially in the formulation of density-pressure coupling. The classical test cases of particle method, a two-dimensional broken dam and forced harmonic oscillated sloshing tank, are selected for a comparative study. The broken dam problem is used for quantitatively compare the SPH and the MPS viscous parameters. The broken dam problem is also used to compare the free surface snapshots of both methods and the corresponding experiment results. In the harmonic oscillated sloshing tank problem, impact pressure at the wall of the tank is investigated. The pressure profile from SPH and MPS method is then qualitatively compared against the corresponding experiments. The strong and weak points of the two particle methods are extensively discussed.

Through the comparative study, several minor differences were observed. MPS is typically computationally more intensive in dealing with large number of particles due to the pressure Poisson equation. In contrast, SPH is computationally more efficient than MPS; however, pressure fluctuation can be problematic in dynamic analysis. Another

problem is observed on the boundary treatment. In the SPH, unphysical gap between fluid particles and wall particles is observed. The unphysical gap is then removed using the newly implemented boundary condition that utilized force balance relation between the wall and fluid particles. No particle penetration is further ensured by introducing the collision model. Because of the absence of shear viscous term in the newly implemented boundary condition formulation, the method perform poorly when violent boundary movement in transversal direction is involved. A dam break case, a sloshing tank case, and a piston wave maker case with physical absorbing layer is modeled using the improved boundary condition. The physical absorbing layer successfully absorbed the incoming wave energy without the need of further mathematical manipulation.

DEDICATION

This thesis is dedicated to my family, especially my Dad, Prof. Dr. Ir. HangTuah Salim, MoCE, who taught me the importance of curiosity and education. Every step I take down this path, brings me closer to you.

ACKNOWLEDGEMENTS

First and foremost, my gratitude goes out to my committee chair Dr. Moo-Hyun Kim, for his direction, advice, and counsel throughout my study. The trust he put in me built my confidence in my own ability to finish this thesis. Additionally, I would like to thank my mentor, Dr. Kyung-Sung Kim, whose experienced insights in the mesh-free Lagrangian CFD are invaluable to this thesis.

Thanks to Dr. Hamn-Ching Chen and Dr. Achim Stössel that served as my committee members and also thought me the fundamentals of CFD through their classes.

Thanks to the Indonesia Endowment Fund for Education (LPDP) for the financial supports that made it possible for me to pursue my degree in the USA. I hope the program can continue to fulfill Indonesian youth's dream.

Thanks to the DualSPHysics and SPHysics developer team, for providing such a good open access SPH source code, and also for the helpful user support. I hope this study can contribute to future SPH developments.

TABLE OF CONTENTS

Page

LIST OF FIGURES

Page

LIST OF TABLES

Page

1. INTRODUCTION

1.1. Computational Fluid Dynamics

The importance of Computational Fluid Dynamics (CFD) to the engineering field cannot be understated in today's world. The capability of CFD to simulate and duplicate many cases at a relatively low cost is one of its many advantages. The nature of typical CFD's solution that discretized time and space continuum into hundreds, if not millions discrete computation points, made it almost humanly impossible for it to solve any complex fluid dynamic's problems without the aid of computers. Therefore, as J.D. Anderson stated in his book (Anderson, 1989), the growth of CFD, and its application to real-world problems, are intimately related to storage and execution speed capability of computer hardware. Combined with a good experiment data, reliable results from CFD simulations can be obtained, and can be used as the benchmark in making key engineering decisions.

The governing equations of fluid dynamics consist of three laws governing transport as following

1. The law of conservation of mass (transport of mass),

$$\frac{D\rho}{Dt} + \rho\nabla.\vec{u} = 0 \qquad (1)$$

2. Newton's second law of motion (transport of momentum),

$$\frac{D\vec{u}}{Dt} = -\frac{1}{\rho}\nabla P + v_0\nabla^2\vec{u} + \vec{F} \qquad (2)$$

3. The first law of thermodynamics (transport of energy)

The present study will focus only on the first and second governing equation. This is done under consideration that the physical quantities that are calculated using the first and second equation (*i.e.*, pressures, impact forces, and the shift of the center of gravity) have more straightforward significance in ocean engineering applications.

1.2. Mesh Free Particle Method

The MPS (Moving Particle Semi-implicit) method and SPH (Smoothed Particle Hydrodynamics) method are computational fluid dynamics' methods that use Lagrangian mesh free framework. The Lagrangian framework differs from its counterpart Eulerian framework in terms of how the physical quantities are calculated. Instead of calculating the flux of certain physical quantities passing through fixed points in space, the Lagrangian framework calculates the physical quantities of fixed fluid masses, as it flows through the spatial dimension. The Lagrangian and Eulerian can be illustrated as in Fig. 1 below.

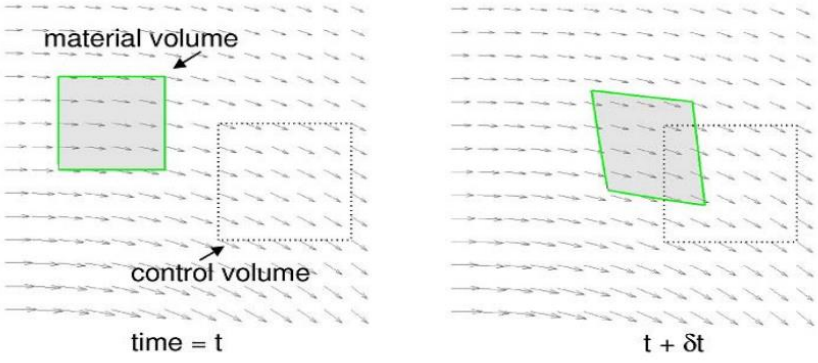

Figure 1: Illustration of Lagrangian framework (solid green line) and Eulerian framework (doted black line), from Price, J.F. (2006)

SPH was first introduced by Gingold and Monaghan (1977), and Lucy (1977), and was initially developed for astrophysics application, while MPS was first introduced by Koshizuka and Oka (1996) and was initially developed for incompressible fluids' simulation. Because SPH was first developed for unbounded computational domain in the astrophysical field, the boundary condition of SPH and its application for incompressible fluid remain interesting to study.

Both methods discretized the fluid continuum into finite fluid particles, and utilize weighted interpolation method to compute the physical quantities of each particle. The discretization of the fluid continuum into mesh free particles can be seen in Fig. 2.

Several notable engineering application that was analyzed using the MPS or SPH methods include, but not limited to, ships' dynamics coupling with liquid sloshing (Kim *et al.*, 2011), wave structure interaction simulation of caisson breakwater (Rogers *et al.*, 2010) and armor type breakwater (Altomare *et al.*, 2014), gravity foundation model with partial flooding chamber (Ulrich *et al.*, 2013), and ship propeller induced scouring (Ulrich *et al.*, 2013), all of which include complex free surface or interface representation.

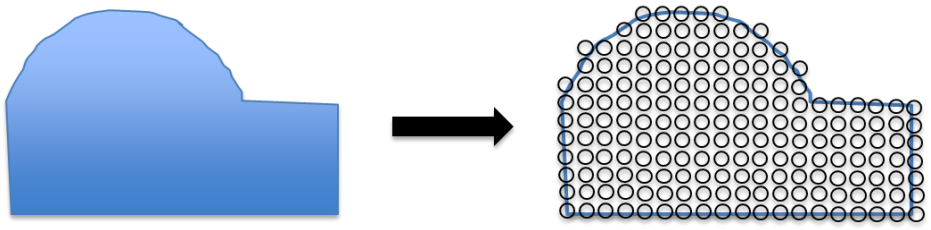

Figure 2: Discretization of the fluid continuum into mesh free particles

Both methods have several notable advantages compared to conventional grid based method, namely having a relatively easy procedure to solve the equation of motions, tracing free surfaces when handling large domains' deformation, and also guaranteeing the conservation of mass. Both of them also suffer from the same disadvantages such as experiencing difficulties in handling diffusion, difficulties in handling impenetrable wall boundary condition, and most importantly, the high computation cost. There are also several other weaknesses and strength that are uniquely possessed by each method, such as impenetrable wall boundary treatment in the SPH, and the higher computation time in MPS due to the implicit step that is use. However, Along with the rapid improvements in computation capabilities in the last several years, new implementations and improvements of SPH and MPS have also emerged. In the present study, the weaknesses and strength of both methods will be studied in details, and some of the issue that is encountered will be addressed with the help of the comparative study.

1.3. Objectives

Three study objectives are formulated based on the similarities of both methods, unique strength and weakness of each method, and also how those qualities can be better understood and improved to better simulate real world fluid dynamics problems. These objectives are:

1. Validating the accuracy and robustness of both SPH and MPS through several test cases

2. Analyzing the general trend, and the unique strength and weakness of each method
3. Improvement of the boundary condition

All three objectives will be analyzed using boundary driven flow cases. This is done under the argument that dynamic pressure acting on structures is one of the most significant physical values for ocean engineering problems, therefore, boundary treatment need to be done correctly in order to get reliable physical values on the boundary.

MPS and SPH program that will be used in present study are:

1. An in-house program from Offshore System Simulation Laboratory, Texas A&M University, USA (Kim *et al.*, 2014), will be used for all MPS simulations
2. An open source GPU-CPU parallel SPH solver DualSPHysics program (Crespo *et al.*, 2015), will be used for initial comparison study using existing model.
3. An open source SPH solver SPHysics program (Gomez-Gesteira *et al.*, 2012a and Gomez-Gesteira *et al.*, 2012b), will be used for SPH model improvement.

The reason that the SPHysics program is used for SPH model improvement instead of DualSPHysics program, is that the SPHysics source code is more practical to alter. This is due to the fact that any alteration on the algorithm of the DualSPHysics program need to take into account the parallelization algorithm, which is beyond the scope of the present study. However, since the mathematical formulations of the two program are

almost identical, the use of both program in the current study will not issue any additional problem.

2. THEORETICAL BACKGROUND

2.1. Integral Representation and its Derivatives

Any arbitrary functions both in MPS and SPH method are represented by weighted average of the physical quantities of its neighboring points, and can be written in mathematical term as,

$$\emptyset(\vec{r}_i) = \int \emptyset(\vec{r}_j) w(|\overrightarrow{r_{ij}}|, r_e)\, dr \qquad (3)$$

Where $\emptyset$ is an arbitrary function, i is the point of interest, j is a neighboring point or an arbitrary point in space, $\vec{x}$ is a position vector in space, $|\overrightarrow{r_{ij}}|$ is the distance between point i and j, r_e is the effective range of particle interaction, and w is the weighting function.

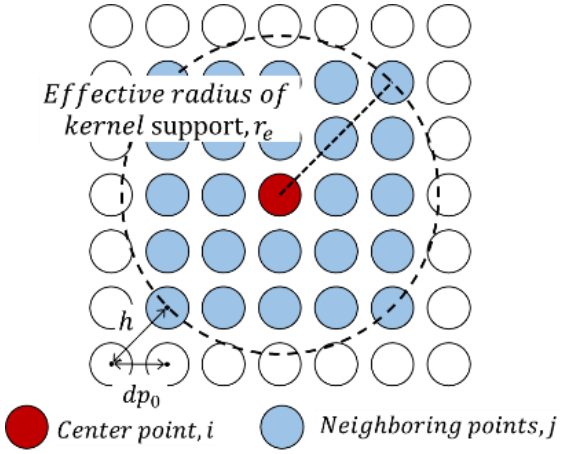

Figure 3: Definition of effective radius of kernel support r_e, point i, and point j, smoothing length h in the SPH method, and initial distance between two neighboring particle dp_o

The neighboring points are defined as the particles that are located within the compact support of the particle of interest, as can be seen in Fig. 3. The discretization of this integral form on both methods is quite different, especially the treatment of the differential operators.

2.2.1. Smoothed Particle Hydrodynamic

In SPH, a relative vector between point i and j is represented as, $\vec{x}_{ij} = (\vec{x}_i - \vec{x}_j)$. The SPH method handles the derivative of a function by analytically differentiating its weighing function. The integral in Equation (3) is discretized into the following form,

$$\emptyset(\vec{x}_i) = \sum \forall_j \emptyset_j w_{ij} = \sum \frac{m_j}{\rho_j} \emptyset_j w_{ij} \quad (4)$$

Where m_j is the particle mass that is calculated using the initial density and volume, ρ_j is the instantaneous particle density, and $\forall_j$ is the instantaneous particle volume. First derivatives in SPH method is handled by analytically differentiating the weighing function as follow,

$$\langle \nabla \emptyset \rangle_i = \sum \frac{m_j}{\rho_j} \emptyset_j \nabla w_{ij} \quad (5)$$

Where ∇w_{ij} is the gradient of the weighing function. To increase the accuracy and simulate the physics correctly, the Equation (5) can have a different form, depending on the equation it applies to. Most notable difference in the formulation of the first derivative in the classical SPH can be seen on the pressure gradient term on the momentum equation (Equation (2)), which will be explained in more detail in later

chapter. Particle support deficiency can be a hindrance when calculating the gradient as well, but can be avoided by renormalizing the weighing function and its gradient as suggested by Bonet and Lok (1999).

Due to its liability to instability and decoupling in the computation, the classical SPH formulation avoids the Laplace operator to be analytically operated on the weighing function (Lo *et al.* 2002). Instead, it combines the Eulerian discretization with the classical SPH first derivative. The discretized Laplace operator in the classical SPH is therefore written as follow,

$$\langle \nabla A \nabla . \vec{\emptyset} \rangle_i = \sum \left[2m_j \frac{\bar{A}_{ij} \vec{r}_{ij} . \vec{\emptyset}_{ij}}{\bar{\rho}_{ij} \left(|\overrightarrow{r_{ij}}|^2 + 0.01h^2 \right)} \nabla w_{ij} \right] \quad (6)$$

Where $\bar{A}_{ij} = (A_i + A_j)/2$ is an average value of arbitrary constants, $\bar{\rho}_{ij}$ is an average density, $\vec{\emptyset}_{ij}$ is arbitrary relative vector between point i and j, $\vec{r}_{ij}$ is relative position vector between point i and j, h is the smoothing length which is defined as the initial distance between two neighboring particle located diagonally from each other, and $0.01{r_e}^2$ is a term to keep the denominator nonzero. Alternative form of Laplacian operator in SPH has been suggested by Schwaiger (2008). It take into account the second order correction of the Laplacian operator. However, due to the complexity and additional computational time that involve n x n matrix inversion in the Schwaiger Laplacian operator, the Laplacian operator that is shown in the Equation (6) will be retained.

2.2.2. Moving Particle Semi-implicit

Several differences in notations involved in the discretization of Integral interpolant and its derivatives between the SPH and MPS need to be addressed beforehand. First of all, a relative vector between point i and j in MPS is represented as, $\vec{x}_{ij} = (\vec{x}_j - \vec{x}_i)$.

Secondly, particle number density is used in the MPS in place of the fluid density. The particle number density the fluids' density in a discretized form. The particle number density is defined as

$$n_i = \sum_{j \neq i} w\left(|\overrightarrow{r_{ij}}|, r_e\right) = \sum_{j \neq i} w_{ij} \quad (7)$$

On the MPS method, discretization of the integral interpolant form of the gradient, divergence, and Laplace operator are done by using the combination between Eulerian discretization and particle interpolant form. No differential operator is to be analytically operated on its weighing function. The gradient, divergence, and Laplace operator in MPS method are expressed as follows

$$\langle \nabla \emptyset \rangle_i = \frac{d}{n^0} \sum_{j \neq i} \frac{(\emptyset_j - \emptyset_i)}{|\overrightarrow{r_{ij}}|^2} \vec{r}_{ij} w_{ij} \quad (8)$$

$$\langle \nabla \emptyset \rangle_i = \frac{d}{n^0} \sum_{j \neq i} \frac{\vec{\emptyset}_{ij}}{|\overrightarrow{r_{ij}}|^2} . \vec{r}_{ij} w_{ij} \quad (9)$$

$$\langle \nabla^2 \emptyset \rangle_i = \frac{2d}{n^0 \lambda_i} \sum_{j \neq i} (\emptyset_j - \emptyset_i) w_{ij} \quad (10)$$

Where $\emptyset$ is an arbitrary scalar, $\vec{\emptyset}$ is an arbitrary vector, d is the number of space dimension, $\vec{r}$ is the coordinate of a particle, n^0 is the initial particle number density, and λ is parameter that is introduced so that the variance increase when quantity is being distributed from particle i to neighboring particle j is equal to the analytical solution. n^0 and λ are defined as follows,

$$n^0 = \max(n_i)\,, when\ t = 0 \quad (11)$$

$$\lambda_i = \frac{\sum_{j \neq i} w_{ij} |\overrightarrow{r_{ij}}|^2}{\sum_{j \neq i} w_{ij}} \quad (12)$$

2.2. Weighing Functions

Although the weighing function of each method has slightly different natures, share several common qualities, such are:

1. Have a compact support, or $w(r_{ij}, r_e) = 0, for\ r_{ij} > r_e$.

   Which means that the particle of interest will only be directly affected by limited number of neighboring particles inside a certain radius.
2. Monotonically decreasing.

   Which means that the closer the neighboring particle to the particle of interest, the more affect will it have on the particle of interest
3. Always have positive value inside compact support, or $w(r_{ij}, r_e) \geq 0, for\ r_{ij} \leq r_e$.

The aforementioned common qualities of both SPH and MPS weighing function is illustrated in the Fig. 4 below.

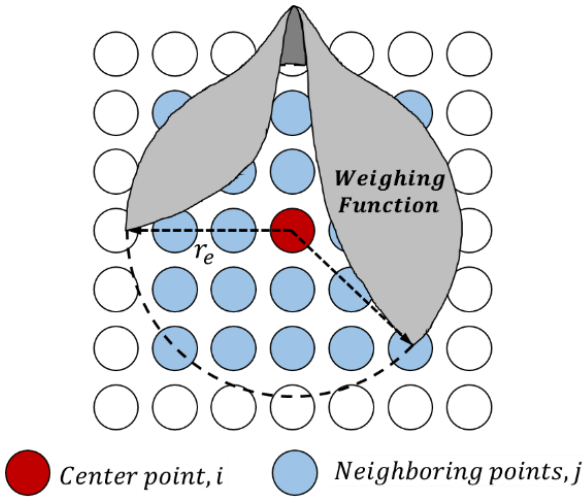

Figure 4: Illustration of a common weighing function

2.2.1. Smoothed Particle Hydrodynamics

Note that since the SPH formulation apply the differential operations directly and analytically on the weighing function, thus the choice of the weighing function has to be done more delicately than in the MPS. In addition to the three properties mentioned before, there are three other important properties that the SPH weighing function have to meet, which are:

1. Normalization, or $\int w\left(|\overrightarrow{r_{ij}}|, r_e\right) dr = 1$
2. Delta function behavior, or $\lim_{r_e \to 0} w\left(|\overrightarrow{r_{ij}}|, r_e\right) dr = \delta\left(|\overrightarrow{r_{ij}}|\right)$, so that as the compact support radius reach zero, each particle qualities is only determined by itself
3. Differentiable to the first order

Described in the next section, is the most commonly used weighing functions (also called kernel functions) in SPH method. The weighing function will be expressed in

term of $q = r/r_e$, and β. Where β acts as the normalization factor, so that the weighing function will be equal to one when integrated.

2.2.1.1 Gaussian

$$w\left(|\overrightarrow{r_{ij}}|, r_e\right) = \beta \begin{cases} \exp(-4\,q^2) & 0 \le q \le 1 \\ 0 & q > 1 \end{cases} \quad (13)$$

Where $\beta = 4/(\pi {r_e}^2)$. The main characteristic of the SPH Gaussian weighing function is that it does not precisely equals to zero when $r = r_e$. The shape of the SPH Gaussian weighing function and its derivative, can be seen in Fig. 5.

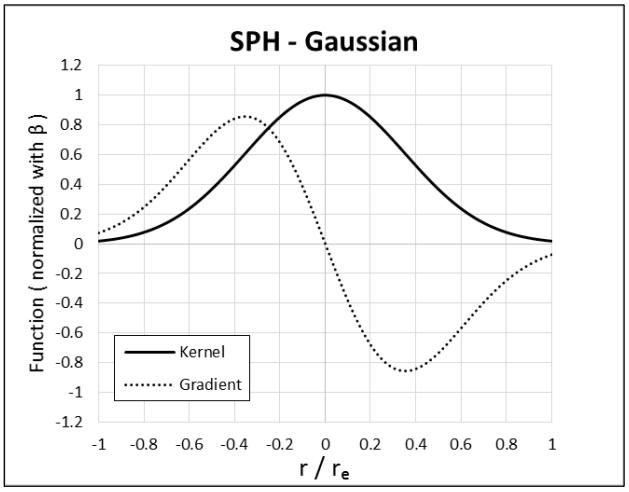

Figure 5: SPH Gaussian weighing function and its derivative

2.2.1.2 Quadratic

$$w\left(|\overrightarrow{r_{ij}}|, r_e\right) = \beta \begin{cases} \frac{3}{4}q^2 - \frac{3}{2}q + \frac{3}{4} & 0 \le q \le 1 \\ 0 & q > 1 \end{cases} \quad (14)$$

Where $\beta = 8/(\pi {r_e}^2)$. The main characteristic of the SPH Quadratic weighing function is that unlike the other three SPH weighing function, the absolute value of its derivative is monotonically increasing as it approaches the center particle. Characteristic as mentioned earlier is desirable because it can prevent particle clustering without any special treatment. The shape of the SPH Quadratic weighing function and its derivative, can be seen in Fig. 6.

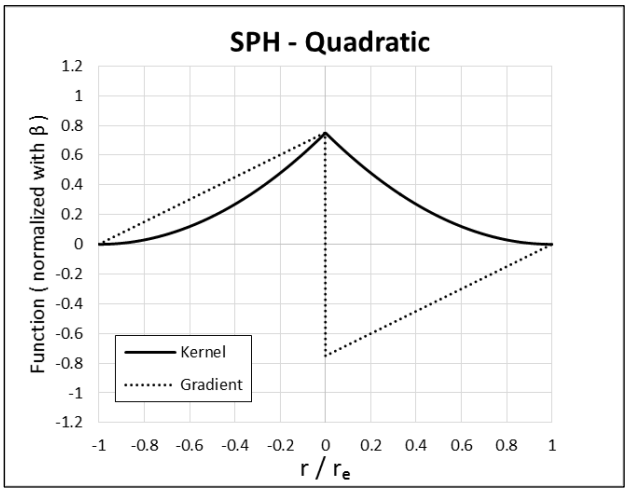

Figure 6: SPH Quadratic weighing function and its derivative

2.2.1.3 Cubic Spline

$$w\left(|\overrightarrow{r_{ij}}|, r_e\right) = \beta \begin{cases} 6q^3 - 6q^2 + 1 & 0 \le q \le 0.5 \\ \frac{1}{4}(2-2q)^3 & 0.5 \le q \le 1 \\ 0 & q > 1 \end{cases} \quad (15)$$

Where $\beta = 40/(7\pi {r_e}^2)$. The SPH Cubic Spline kernel shows a close resemblance with the SPH Gaussian kernel, in a way that both has a wider shape feature. However, different from the Gaussian function, the SPH Cubic Spline function is exactly zero

when $r = r_e$. The SPH Cubic Spline is smoother if compared to the SPH Quadratic weighing function because it comprised of higher order polynomial terms. The shape of the SPH Cubic Spline weighing function and its derivative, can be seen in Fig. 7.

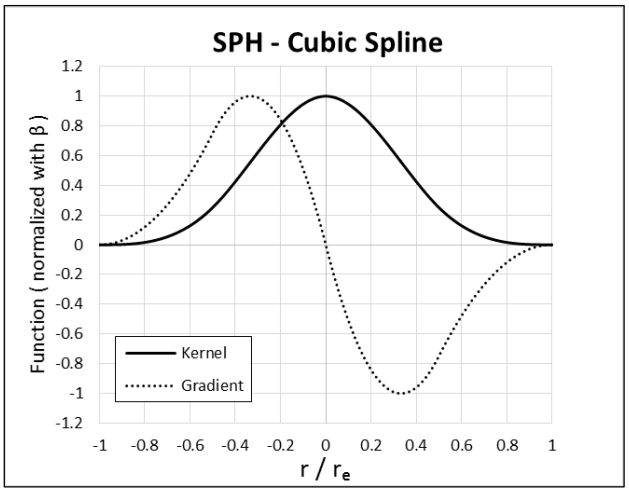

Figure 7: SPH Cubic Spline weighing function and its derivative

2.2.1.4 Quintic

$$w\left(|\overrightarrow{r_{ij}}|, r_e\right) = \beta \begin{cases} (1-q)^4\,(4q+1) & 0 \le q \le 1 \\ 0 & q > 1 \end{cases} \qquad (16)$$

$\beta = 7/(\pi {r_e}^2)$. The main characteristic of the SPH Quintic weighing function, is that it gives the best trade off balance between the accuracy and computation time (Crespo, 2008). Furthermore, it remain the highest order and widely use polynomial weighing function in the SPH method. The shape of the SPH Quintic weighing function and its derivative, can be seen in Fig. 8.

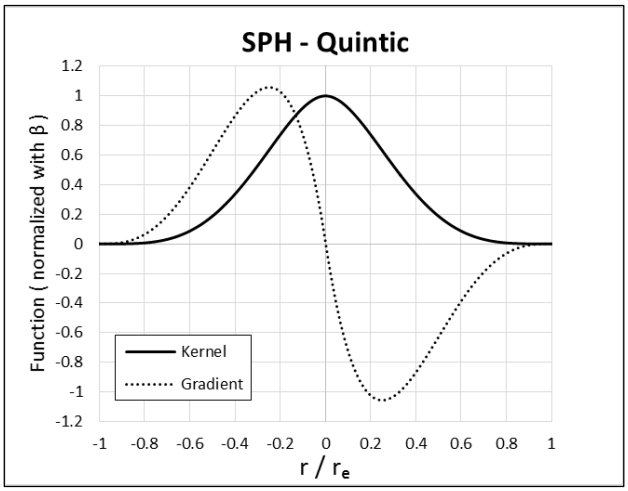

Figure 8: SPH Quintic weighing function and its derivative

Notice that other than the quadratic weighing function, the weighing function's gradients goes to zero near the center particle. This particular feature might cause particle clustering, which also known as tensile instability problem. The problem can be solved by introducing additional repulsive term on the pressure term such as explained in detail by Monaghan (2000). The magnitude of the additional repulsive term, or also called the tensile correction, varies depends on the weighing function that is being used, and can be found in Crespo (2008).

2.2.2. Moving Particle Semi-implicit

There are three widely used MPS weighing functions in the MPS. As mentioned by Lee et.al, (2011), these weighing functions are MPS Koshizuka 1996 (Equation (17)), MPS Gaussian (Equation (18)), and MPS Sextic (Equation (19)) weighing function. The weighing functions are expressed as below,

$$w\left(|\overrightarrow{r_{ij}}|, r_e\right) = \begin{cases} \frac{1}{q} - 1 & 0 \le q \le 1 \\ 0 & q > 1 \end{cases} \quad (17)$$

$$w\left(|\overrightarrow{r_{ij}}|, r_e\right) = \begin{cases} \exp(-6.3\, q^2) & 0 \le q \le 1 \\ 0 & q > 1 \end{cases} \quad (18)$$

$$w\left(|\overrightarrow{r_{ij}}|, r_e\right) = \begin{cases} (1-q)^3\,(1+q)^3 & 0 \le q \le 1 \\ 0 & q > 1 \end{cases} \quad (19)$$

These weighing functions can be seen in Fig. 9 below.

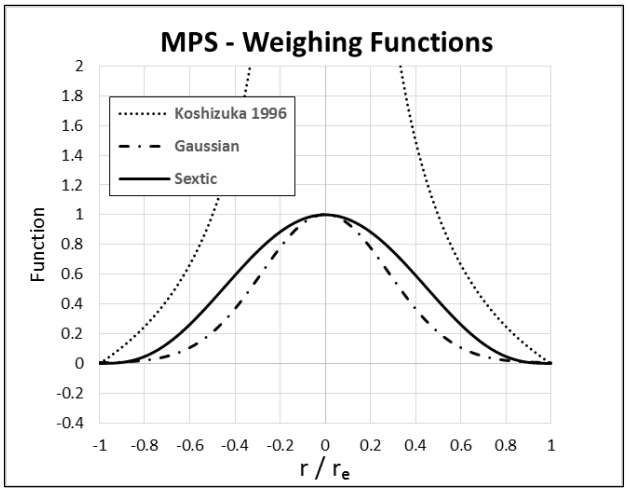

Figure 9: MPS Weighing functions

The Koshizuka 1996 weighing function has a distinctive characteristic of going to infinity as $r \to 0$. This feature provide a better numerical stability in the model of incompressibility (Koshizuka & Oka, 1996). However, the neighboring particles value that is close to the edge of r_e, will still highly affecting the center particles value, a lot greater than the other two weighing functions. On the other hand, just like the SPH Gaussian (Equation (18)) weighing function, the MPS Gaussian weighing function does not precisely equal to zero as $r = r_e$.

2.3. Density

2.3.1. Smoothed Particle Hydrodynamics

Originally, density calculation in the SPH was done by directly using Equation (4). However, because of the lack of particle support, which defined as the particles that located within the compact support, near edges and interfaces, the use of Equation (4) directly can lead to substantial truncation errors. One solution that can be adopted by normalizing the density summation function such as proposed by Randles and Libersky (1996) below,

$$\rho_i = \frac{\sum m_j w_{ij}}{\sum \frac{m_j}{\rho_j} w_{ij}} \qquad (20)$$

The fluid density from Equation (20) need to be calculated before others physical quantities can be calculated, therefore, it requires an additional loop over all the fluid particles. However, even after the modification, the density will still give erroneous results, particularly for unbounded fluid flow. Another formulation of density calculation that can avoid aforementioned problems is formulated by manipulating the continuity equation as follows,

$$\frac{d\rho}{dt} = -\rho \nabla . \vec{u} = \vec{u} . \nabla \rho - \nabla . (\vec{u} \rho)$$

Rewriting the equation using SPH notations,

$$\frac{d\rho_i}{dt} = \sum m_j \vec{u}_{ij} \nabla w_{ij} \qquad (21)$$

Equation (21) calculate the change of density over time instead of calculating it directly, and can be computed in the same loop with other physical quantities. Equation (21) is also more preferable for problems with high discontinuity such as impact pressure problems (Liu & Liu, 2003).

In the present study, both density formulation of Equation (13) and (14) are used. While the Equation (14) is used for every time steps, the Equation (13) is applied every N time steps. The use of Equation (13) on every N time steps, is also called Shepard density filter.

2.3.2. Moving Particle Semi-implicit

In the MPS, the density is proportional to the particle number density n_i. It can be expressed in a mathematical formulation as,

$$\rho_i = m\, N_i = \frac{m\, n_i}{\int w\left(|\overrightarrow{r_{ij}}|, r_e\right) dr} \qquad (22)$$

Where ρ_i is the particle density, m is the particle mass, N_i is number of particles in a unit volume, and the denominator is the analytic integral of the weighing function. However, since the particle number density is proportional to particle density, it is more practical if all the MPS governing equations are formulated in term of n_i, instead of ρ_i, to avoid unnecessary additional computation step.

2.4. Velocities from Navier-Stokes Equation

2.4.1. Smoothed Particle Hydrodynamics

Recalling the pressure gradient term on the right hand side of Equation (2), the use of SPH gradient term such as on Equation (5) is avoided because it does not conserve linear and angular momentum exactly. Instead, by employing product rule on the pressure gradient term, one can formulate the symmetrized form of pressure gradient term as below,

$$\nabla\left(\frac{P}{\rho}\right) = \frac{\rho\nabla P - P\nabla\rho}{\rho^2}$$

$$\frac{1}{\rho}\nabla \mathrm{P} = \nabla\left(\frac{P}{\rho}\right) + \frac{P\nabla\rho}{\rho^2}$$

Rewriting the equation in SPH notation,

$$\langle\frac{1}{\rho}\nabla P\rangle_i = -\sum_{j\in R}\left[m_j\left(\frac{P_i}{\rho_i^2} + \frac{P_j}{\rho_j^2}\right)\nabla w_{ij}\right] \qquad (23)$$

There are several ways to treat the diffusion term of the momentum equation, but the most widely used is the artificial viscosity formulation. Monaghan (1994) first introduced the artificial viscosity to handle problems involving strong shocks. This artificial viscosity produces bulk and shear viscosity, and also guarantees conservation of angular momentum (Monaghan, 1992). However, for problems involving bounded fluid edge, low velocities, or shocks in low viscosity fluid, this artificial viscosity may give inaccurate results (Morris *et al.*, 1997). The artificial viscosity is expressed as,

$$\langle v_0 \nabla^2 \vec{u} \rangle_i = \begin{cases} \sum_{j \in R} \left[m_j \frac{\alpha \bar{c}_{ij} h}{\bar{\rho}_{ij}} \frac{\vec{r}_{ij}.\vec{u}_{ij}}{\left(\left| \overrightarrow{r_{ij}} \right|^2 + 0.01h^2 \right)} \nabla w_{ij} \right] & if\ \vec{r}_{ij}.\vec{u}_{ij} \\ 0 & otherwise \end{cases} \quad (24)$$

Where α is free parameter that need to be adjusted for respective problems, taking into consideration that the effect of artificial viscosity on global solution should be negligible while still ensuring sufficient damping of spurious pressure oscillations (Adami et.al, 2012). Furthermore, Monaghan (1992) suggested that α should be near 1 for best result. Adami et.al (2012) stated that for 2D fluid simulations, an equivalent physical viscosity for a given artificial viscosity can be formulated as follows,

$$v_0 = \frac{1}{8} \alpha \bar{c}_{ij} h \quad (25)$$

By keeping the speed of sound near constant, which means satisfying the pseudo incompressibility condition, the equivalent physical viscosity can be assumed to be constant. There are several other ways to formulate the momentum diffusion term on the SPH method, namely the laminar viscosity and sub-particle scale (SPS) turbulence formulation (Rogers and Dalrymple, 2004 & Dalrymple and Rogers, 2006). However, the artificial viscosity will be used in the present study due to its simplicity and vast availability of references for data validation.

By definition, the rate of change of particle position is $\frac{D\vec{x}_i}{Dt} = \vec{u}_i$. However, Monaghan (1992) stated that it is necessary for free surface problems, the rate of change of particle position should be formulated using XSPH variant as follows,

$$\frac{d\vec{x}_i}{dt} = \vec{v}_i + \varepsilon \sum_{j \in R} \left[m_j \vec{u}_{ij} \nabla w_{ij} \right] \quad (26)$$

This XSPH formulation contribute to prevent the particles to be penetrated one another, also help to keep the continuity of the fluid motion. Monaghan (1989) proved that Equation (26) does not introduce an artificial diffusion. However, it does introduce an artificial dispersion.

2.4.2. Moving Particle Semi-implicit

In the MPS method, the conservation of momentum equation (Equation (2)) is splitted into two parts. The first part, which is called the explicit time step, consist of diffusion and applied forces terms. The aforementioned terms are solved explicitly to obtain physical quantities on the intermediate time step $k + \frac{1}{2}$ as follow,

$$\frac{d\vec{u}}{dt} = \frac{\vec{u}^{k+\frac{1}{2}} - \vec{u}^{k}}{\Delta t} = \upsilon_0 \nabla^2 \vec{u} + \vec{F}$$

$$\vec{u}^{k+\frac{1}{2}} = \upsilon_0 \nabla^2 \vec{u}^{k} \Delta t + \vec{F}^{k} \Delta t + \vec{u}^{k} \quad (27)$$

Here Δt is the time step, $\vec{u}^{k+\frac{1}{2}}$ is the intermediate velocity, υ_0 is the fluids' kinematic viscosity, and $\vec{F}^{k}$ is the applied force. The diffusion term on the right-hand side of Equation (27) can be rewritten in MPS notation such as formulated in Equation (10). Depends on the algorithm that is used, particles can then be distributed using the intermediate velocity to obtain intermediate particle position vectors,

$$\vec{x}^{k+\frac{1}{2}} = \vec{x}^{k} + \vec{u}^{k+\frac{1}{2}}\Delta t \qquad (28)$$

From the intermediate position vectors $\vec{x}^{k+\frac{1}{2}}$, one can calculate the intermediate particle number density $n^{k+\frac{1}{2}}$. These intermediate physical quantities are then used on the second part of the conservation of momentum equation.

The second part of the conservation of momentum equation, which is called the implicit time step, consist of the pressure gradient term of the conservation of momentum equation. This pressure term is solved implicitly along with the conservation of mass equation (Equation (1)) to satisfy the incompressibility condition. The resulting pressure and density coupling will be discussed in detail later.

2.5. Density and Pressure Coupling

2.5.1. Smoothed Particle Hydrodynamics

Classical SPH method treated the supposedly incompressible fluid as a weakly compressible fluid. Therefore, slight density variation from its original value is permitted. Morris et.al. (1997) proposed that the density fluctuation should be kept within 3% of its original value. This requirement is needed to satisfy the quasi-incompressibility condition of the fluid while allowing larger time steps to be used for practicality at the same time.

The weakly compressible treatment enables the equation of state that relates the density to pressure to be used. The calculation of the pressure can be done after the new density distribution is updated. The equation of state is expressed as follows,

$$P = B\left[\left(\frac{\rho}{\rho_0}\right)^{\gamma} - 1\right] \quad (29)$$

Where $B = c_0^2\rho_0/\gamma$ is the bulk modulus of the fluid, ρ_0 is the reference density, c_0 is the speed of sound at the reference density. Typically, c_0 is chosen to be 6-10 times $|\vec{v}_{max}|$ to keep the density variation within 1%-3% of the original density. γ is a parameter that controls the pressure response to the density variation and is typically chosen to be 7.

The instantaneous speed of sound is defined as ${c_s}^2 = \partial P/\partial\rho$. Since the bulk modulus of the fluid is constant, the speed of sound will change when the density is changing. The relation between the instantaneous speed of sound c_s and instantaneous fluid density ρ can be derived from Equation (29) as follows,

$$c_s = c_0\left(\frac{\rho}{\rho_0}\right)^{\frac{\gamma-1}{2}} \quad (30)$$

From Equation (30), it can be seen that If the density variation is kept within $n\%$ threshold, the speed of sound will have $\sim 3n\%$ variation from its original value.

The equation of state allows the SPH method to be solved in a entirely explicit manner, thus greatly saves computation time. On initial studies, the pseudo compressibility introduced in the equation of state may cause nonphysical negative pressure if the c_0 is not carefully chosen.

Another problem related to the usage of the equation of state comes from the power relation between the pressure and density. Small errors in density may cause an

exponentially larger errors in the pressure, especially for low Reynolds number flows (Morris *et al.*, 1997). This explicit pseudo incompressibility modeling and the use of the equation of state, remain to be the most prominent characteristic of the classical SPH formulation.

2.5.2. Moving Particle Semi-implicit

Since particle number density is proportional to density, Equation (1) can be rewritten as,

$$\frac{dn}{dt} = \frac{n^0 - n^{k+\frac{1}{2}}}{\Delta t} = \frac{n'}{\Delta t} = -n^0 \nabla . \vec{u}' \qquad (31)$$

Where $n^{k+\frac{1}{2}}$ is the intermediate particle number density, defined as the particle number density calculated after all particles were distributed by forces other than pressure induced force.

On the MPS method, the pressure induced velocity is calculated separately, after the velocity induced by other body forces and surface forces is applied. The pressure induced velocity $\vec{u}'$ can be obtained from,

$$\frac{d\vec{u}}{dt} = \frac{\vec{u}'}{\Delta t} = -\frac{1}{\rho^0} \nabla P \qquad (32)$$

Where ρ^0 is the reference density. By combining Equation (31) and (32), one can construct a Pressure Poisson equation as below

$$\langle \nabla^2 P \rangle_i^k = -\frac{\rho^0}{\Delta t} \nabla . \vec{u}' = \frac{\rho^0}{\Delta t^2} \frac{n^0 - n^{k+\frac{1}{2}}}{n^0} \quad (33)$$

By substituting the left-hand side of Equation (33) with Equation (10), one can solve for pressure implicitly using linear matrix solver. Tanaka et.al (2010) proposed that divergence free condition should be imposed on the source term, along with conservation of particle number density condition to stabilized the computation. The aforementioned proposed algorithm has been proven to save computational time because particle position and particle number density does not need to be updated on the intermediate time step (Lee *et al.*, 2011). The source term is expressed as

$$\langle \nabla^2 P \rangle_i^k = (1-\gamma) \frac{\rho^0}{\Delta t} \nabla . \vec{u}_i^{k+\frac{1}{2}} + \gamma \frac{\rho^0}{\Delta t^2} \frac{n^0 - n_i^k}{n^0} \quad (34)$$

Where n^k is the particle number density from the current time step, and γ is the relaxation coefficient with a typical value of 10^{-3} (Tanaka *et al.*, 2010). Note that for this source term formulation, the particle does not need to be redistributed after the explicit terms calculation, thus greatly saves computation time. As proposed by Koshizuka and Oka (1996), it is common to use larger smoothing length when solving the pressure Poisson equation for better accuracy. More detailed derivation of the fundamentals of the MPS method are explained in Koshizuka and Oka (1996)

2.6. Boundary Treatment

2.6.1. Smoothed Particle Hydrodynamics

There are three proponent methods in treating impenetrable wall boundary in SPH. These three methods are dynamic boundary method, ghost particles method, Repulsive particles method. The SPH boundary conditions mentioned above can be illustrated by Fig. 10 bellows.

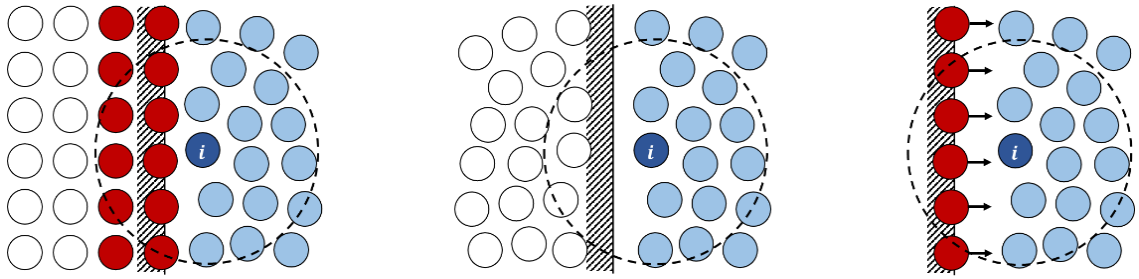

Figure 10: Dynamic boundary method (left), ghost particle method (center), and repulsive particles method (right) on SPH model

Much like boundary treatment on the MPS, the dynamic boundary method, treated boundary particles as a fixed particle, or a particle with a prescribed motion that have the same physical properties as the fluid particles. This treatment means that when fluid particles approach the wall particles, the density of the wall particles will increases according to Equation (21), and thus increase the repulsive pressure exerted by the wall particles. More than one layer of wall particles can be used to ensure that no fluid particles can penetrate. Dummy particles are often used this method as well, to increase the particle support that is needed to achieve better interpolation accuracy. This method has the advantages of having uncomplicated formulation and calculations can be done

inside the same loop as the fluid particles, thus giving this method high parallelization capability.

However, because the pressure exerted by the boundary particle on the dynamic particles method is calculated using the equation of state, their pressure is not directly linked to the surrounding fluid particles pressure. Furthermore, when used with Equation (21), the dynamic particles method will cause an unphysical gap between wall particles and fluid particles to emerge, such as shown in Fig. 11. This gap appears mainly due to the velocity discontinuity experienced by the wall particles lead to density discontinuity, and thus, pressure calculated using this method tend to be significantly exaggerated. Nevertheless, when density is calculated with Equation (20), there will be fluid particles that can penetrate the wall particles, especially on a boundary with sharp edges.

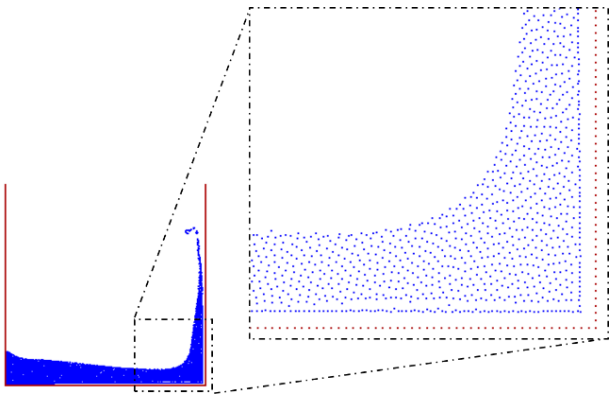

Figure 11: Unphysical gap on SPH boundary

The ghost particles method works by generating a mirror image of the oncoming fluid particles in every time step. The ghost particle will be generated when the distance between the fluid particle and the wall becomes smaller than r_e, and will be erased

otherwise. The ghost particles will have the same physical quantities with its image. However, just like the dynamic particle method, ghost particle method facing significant difficulties in handling complex geometries. Furthermore, due to the calculation of ghost particle positions and its physical quantities, it will be computationally more expensive and complicated.

On repulsive particle method, wall particles exert an artificial force to oncoming fluid particles, similar to the Lenard Jones Potential force. The interaction between the wall particle and the oncoming fluid particle is two-body interaction, instead of the integral interpolant interaction. The value of the repulsive force of the wall particles is not linked to the properties of the fluid, and tend to cause unphysical gap such as seen in Fig. 11 as well.

Among all three proponent boundary treatment on the SPH, this study will use dynamic boundary method as the benchmark formulation. Furthermore, the inexistence of any direct relations between fluid particles pressure and the wall pressure in this particular method will be highlighted. It is hypothesized that if any direct relation between the two can be formulated, one can directly use the pressure of the wall particle to estimate the dynamic pressure acting on it, an option which is not available in the current solver. It can also remove the unphysical gap appeared on the dynamic particles and repulsive particles methods.

2.6.2. Moving Particle Semi-implicit

On the MPS method, impenetrable wall boundary condition is satisfied automatically according to Equation (33). When fluid particles approach wall particles, the divergence and the particle number density of the wall particles will increase, thus increasing pressure in that area, keeping the oncoming fluid particles to penetrate through the wall.

Dummy particles are commonly used on the MPS wall boundary so that particles located near or on the boundary have sufficient number of particles support. The dummy particles should not be included in the Poisson pressure calculation, and their pressure are set to zero. See Fig. 12 to better understand dummy and wall particles configuration on MPS.

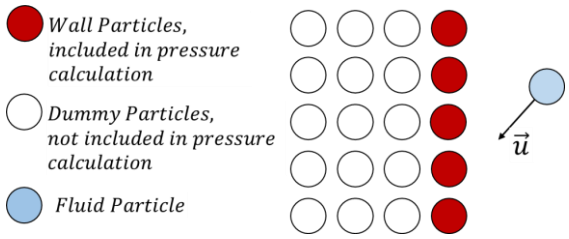

Figure 12: Particles configuration on MPS boundary

Collision model is used to further ensuring that no fluid particle can penetrate the wall boundary. It imitates the transfer of momentum between two collided solid body, according to the Newton's Third Law of Motion. The illustration can be seen in Fig. 13 below.

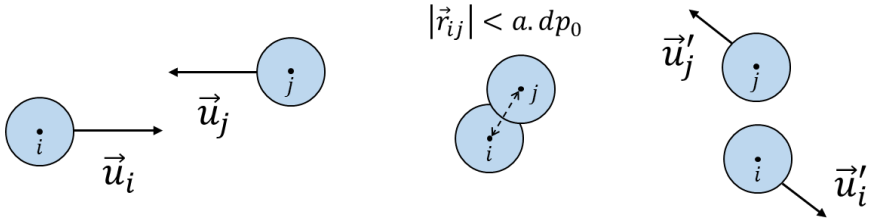

Figure 13: Collision model mechanism on the MPS

The new particle velocity after collision is formulated as,

$$\vec{u}_i' = \vec{u}_i + \frac{(1+b)}{2}(\vec{u}_{ij}.\vec{e}_{ij})\vec{e}_{ij} \quad (35)$$

Where $\vec{e}_{ij}$ is the unit vector between the colliding particle, and can be written as $(\vec{x}_i - \vec{x}_j)/|\vec{r}_{ij}|\hat{\imath} + (\vec{z}_i - \vec{z}_j)/|\vec{r}_{ij}|\hat{\jmath}$. Both a and b are numerical parameters, where a is the coefficient that determined the minimum activation range of the collision model, and b is the elasticity ratio. Lee et.al (2012) suggested that $a = 0.97$ and $b = 0.2$ should be used on the MPS collision model for best result. Furthermore, the collision model had proved to improve the stability of the MPS model, as discussed in details in Lee et.al (2011).

Free surface boundary condition is satisfied by setting the pressure $P = 0$ on free surface particles when solving Equation (33). A particle is considered as a free surface particle when it satisfies both conditions below (Lee et.al, 2011),

$$n_i^k < \beta_1 n^0 \quad (36)$$

$$N_i^k < \beta_2 N^0 \quad (37)$$

Where N is the number of neighboring particle within r_e, β_1 and β_2 are parameters below 1.0 with typical value of 0.97 and 0.85 respectively (Kim *et al.*, 2014).

2.7. Time Integration Algorithm

2.7.1. Smoothed Particle Hydrodynamics

Variable time step discretization is used for stability. It is dependent on the forcing term, and the combination between Courant-Friedrich-Levy condition and viscous diffusion term (Monaghan *et al.*, 1989)

$$\Delta t = CFL\,.\min(\,\Delta t_{cv}, \Delta t_f\,) \tag{38}$$

$$\Delta t_{cv} = min_i \frac{h}{c_{s,i} + max_j \left| \frac{h\,\vec{u}_{ij}.\vec{r}_{ij}}{|\overrightarrow{r_{ij}}|^2} \right|} \tag{39}$$

$$\Delta t_f = min_i \sqrt{h/|f_i|} \tag{40}$$

Where CFL is coefficient ranging from 0.1 – 0.5, $|f_i|$ is force per unit mass on particle i. Two time integrator scheme are implemented in the present study: (i) the Predictor-Corrector Scheme (Monaghan, 1989), and (ii) Verlet (Verlet, 1967). For simplicity, define:

$$\frac{d\vec{u}_i}{dt} = \vec{F}_i \tag{41}$$

$$\frac{d\vec{r}_i}{dt} = \vec{V}_i \quad (XSPH\ correction\ eq(19)\ included) \tag{42}$$

$$\frac{d\rho_i}{dt} = D_i \tag{43}$$

2.7.1.1 Predictor Corrector Scheme

The predictor corrector scheme divide each full time step into two steps, predictor and corrector step. The scheme is relatively more computationally expensive and is accurate to $O(\Delta t^2)$. The scheme had been used to show that the SPH method conserves both linear and angular momentum (Crespo, 2008).

The predictor step follows the following algorithm,

$$\vec{u}_i^{k+1/2} = \vec{u}_i^k + \vec{F}_i^n \frac{\Delta t}{2} \quad (44)$$

$$\vec{r}_i^{k+1/2} = \vec{r}_i^k + \vec{V}_i^k \frac{\Delta t}{2} \quad (45)$$

$$\rho_i^{k+1/2} = \rho_i^k + D_i^k \frac{\Delta t}{2} \quad (46)$$

After the density at intermediate time step is calculated, intermediate pressure $P_i^{k+1/2} = f\left(\rho_i^{k+1/2}\right)$ is calculated using Equation (29). Using the previously calculated values, the intermediate values is then corrected as follow,

$$\vec{u}_i^{k+1/2} = \vec{u}_i^k + \vec{F}_i^{k+1/2} \frac{\Delta t}{2} \quad (47)$$

$$\vec{r}_i^{k+1/2} = \vec{r}_i^k + \vec{V}_i^{k+1/2} \frac{\Delta t}{2} \quad (48)$$

$$\rho_i^{k+1/2} = \rho_i^k + D_i^{k+1/2} \frac{\Delta t}{2} \quad (49)$$

Without updating the pressure, the corrected intermediate values are then used to calculate the new values for the next time step,

$$\vec{u}_i^{k+1} = 2\vec{u}_i^{k+1/2} - \vec{u}_i^k \quad (50)$$

$$\vec{r}_i^{k+1} = 2\vec{r}_i^{k+1/2} - \vec{r}_i^k \quad (51)$$

$$\rho_i^{k+1} = 2\rho_i^{k+1/2} - \rho_i^k \quad (52)$$

Finally, the pressure at the next time step $P_i^{k+1} = f\left(\rho_i^{k+1}\right)$ is calculated using Equation (29).

2.7.1.2 Verlet Scheme

The Verlet scheme use two previous points in time instead of just one. The evolution of position in time take into account the acceleration in addition to the velocity. In general, the variables are calculated as follow,

$$\vec{u}_i^{k+1} = \vec{u}_i^{k-1} + \vec{F}_i^k 2\Delta t \quad (53)$$

$$\vec{r}_i^{k+1} = \vec{r}_i^k + \vec{V}_i^k \Delta t + \vec{F}_i^k \frac{\Delta t^2}{2} \quad (54)$$

$$\rho_i^{k+1} = \rho_i^{k-1} + D_i^k 2\Delta t \quad (55)$$

The pressure at the next time step $P_i^{k+1} = f\left(\rho_i^{k+1}\right)$ is calculated using Equation (29). To stop the time integration to diverge, once every M time steps, values at step k is used instead of values at step k-1.

2.7.2. Moving Particle Semi-implicit

Recalling Equations (20), (21), (25), and (27), time stepping in the MPS can be summarized as follow:

1. Search for neighboring particle, and calculate n_i^k

2. Update intermediate velocity due to external forces and viscous term explicitly,

   $$\vec{u}_i^{k+1/2} = v_0 \nabla^2 \vec{u}_i^k \Delta t + \vec{F}_i^k \Delta t + \vec{u}_i^k$$

3. From the Poisson Pressure equation, solve for P_i^k,

   $$\langle \nabla^2 P \rangle_i^k = (1-\gamma)\frac{\rho^0}{\Delta t} \nabla . \vec{u}_i^{k+1/2} + \gamma \frac{\rho^0}{\Delta t^2} \frac{n^0 - n_i^k}{n^0}$$

4. Update final velocity from the pressure gradient,

   $$\vec{u}_i^{k+1} = -\frac{1}{\rho^0} \nabla P_i^k \Delta t + \vec{u}_i^{k+1/2}$$

5. Update the particles position,

   $$\vec{r}_i^{k+1} = \vec{r}_i^k + \vec{u}_i^{k+1} \Delta t$$

6. Apply the collision model correction,

   $$\vec{u}_i^{k+1} = \vec{u}_i^{k+1} + \vec{u}_i^{Coll}$$

   $$\vec{r}_i^{k+1} = \vec{r}_i^{k+1} + \vec{u}_i^{k+1} \Delta t$$

7. Go to the next time step

3. COMPARATIVE STUDY ON MPS AND CLASSICAL SPH FOR FLUID FLOW WITH VIOLENT FREE SURFACE*

In order to see more clearly the underlying characteristics of each method, a comparative study needs to be done using a typical test case, with the most similar setting for each method. Dynamic boundary condition method is used in the SPH method because of its resemblance to the MPS boundary condition.

Dam break case and forced-oscillated sloshing tank case are used in this study. A quantitative study is conducted for the fluids' leading-edge and free surface representations of the dam break case, while a qualitative study is carried out for the pressure profile of the sloshing test case. An in-house program from Offshore System Simulation Laboratory, Texas A&M University, USA is used for the MPS simulations (Kim *et al.*, 2014), while for SPH simulations, an open source parallel SPH solver DualSPHysics program is used (Crespo *et al.*, 2015).

From this study, it is intended that one can have a better understanding of the general trend, and the strong and weak points of both methods. The underlying principles behind those strengths and weaknesses, and possible ideas for improvements are also briefly discussed.

* Reprinted with permission from "Comparative Study on Particle Method for Numerical Simulation," by Bakti, F.P., Kim, K.S., Kim, M.H., Park, J.C., 2015. *Int. Soc. of Offshore and Polar Eng. Proc.* vol. 3, 424-431, Copyright [2015] by International Society of Offshore and Polar Engineers

3.1. Dam Break Case

A dam break case is used to compare MPS, SPH, and experiment results both quantitatively and qualitatively. A quantitative comparison is done by studying the effect of viscosity on the leading edge of the fluids' flow. A qualitative study will be done by studying the fluids' free surface representation. The case setup that is used is the same as the one in Koshizuka and Oka (1996), and can be seen in the Fig. 14 and Table 1

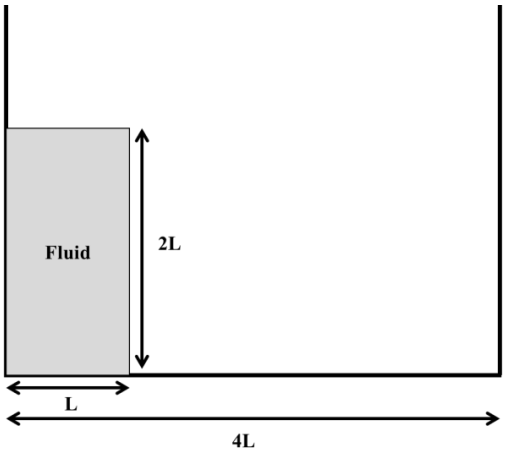

Figure 14: Dam break case configuration

The choice of c_o = 85 m/s that is used in SPH model has successfully kept the density variation within the 1% range from its original value. The characteristic of each model's formulation, especially on its viscosity and boundary condition, is studied using several different viscosity coefficients while keeping other parameters constant. The artificial viscosity is used for the SPH model while a typical kinematic viscosity is used for the MPS model. Five different viscosity values are used in both methods, and can be seen in Table 2. Table 2 also shows the corresponding hypothesized equivalent kinematic viscosity value for each artificial viscosity coefficient that is used, based on Eq. (25).

Table 1: Parameters used in dam break case

General	
Simulation time	3 sec
L	0.15 m
ρ_o	1000 kg/m3
G	9.81 m/s2
dp_o	0.00375 m
Number fluid of particles	3200 particles
MPS	
Effective range of compact support, r_e	
Particle number density	$2.1dp_o$
Laplacian	$4.1dp_o$
Weighing function, $w(r, r_e)$	$w(r,r_e) = \begin{cases} \left(1-\frac{r}{r_e}\right)^3\left(1+\frac{r}{r_e}\right)^3, & if\ 0 \le r < r_e; \\ 0, & otherwise \end{cases}$
SPH	
Reference Speed of sound, c_o	85 m/s
Effective range of compact support, $2r_e$	$2\sqrt{2}dp_o$
Weighing function, $w(r, r_e)$	$w(r,r_e) = \begin{cases} \left(1-\frac{r}{2r_e}\right)^4\left(\frac{2r}{r_e}+1\right), & if\ 0 \le r < 2r_e; \\ 0 & otherwise \end{cases}$

Table 2: Dam break simulation case for MPS and SPH model, for leading edge comparison

MPS	SPH	
υ_0	α_o	Hypothesized Equivalent υ_0 ($\upsilon_0 = \frac{1}{8}\alpha_0 \bar{c}_{ij} h$)
1.00x10^{-6}	1.08x10^{-5}	1.00x10^{-6}
1.00x10^{-5}	1.08x10^{-3}	1.00x10^{-4}
1.00x10^{-4}	1.08x10^{-1}	1.00x10^{-2}
1.00x10^{-3}	3.00x10^{-1}	2.78x10^{-2}
1.00x10^{-2}	5.38x10^{-1}	5.00x10^{-2}

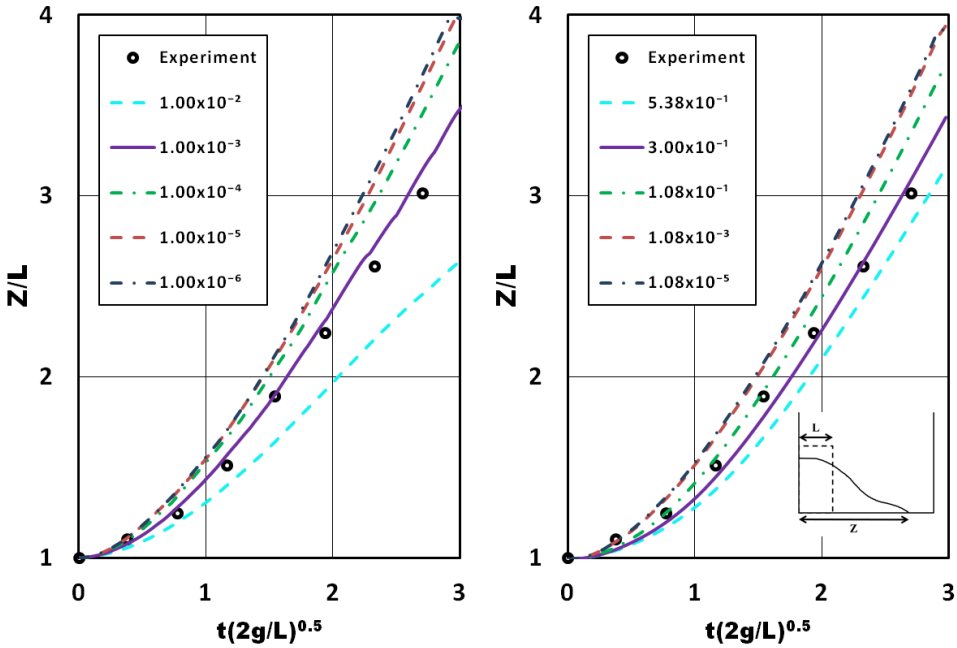

Figure 15: Dam break case leading edge of MPS for various kinematic viscosity values υ_0 (left) and SPH for various artificial viscosity coefficient values α_0 (right), experiment result is taken from Koshizuka & Oka (1996)

From Fig. 15, it can be seen that when the the flow is considered inviscid i.e. $\upsilon_0 < O(10^{-4})$ for MPS and $\alpha < O(10^{-1})$ for SPH, the overall leading velocities for both methods are almost the same. It can also be observed that the artificial viscosity in the

SPH model begins to significantly affect the leading edge profile and the leading velocity, when its α approaches $O(10^{-1})$ which is assumed to be equivalent to υ_0 of the order of $O(10^{-2})$. On the MPS model, the leading edge profile begins to be affected by kinematic viscosity value higher than $O(10^{-3})$. On overall, the MPS method has a higher sensitivity to viscosity than the SPH method. The formula $\alpha_o = 8\upsilon_0/h\bar{c}_{ij}$ will need to be modified if a good relation between the kinematic viscosity value on MPS and the artificial viscosity coefficient value on the SPH is to be calculated. This relation is needed to obtain better objectivity for a comparative study of the two methods. From our simulation results, it is found that the kinematic viscosity value υ_0 in the range of $10^{-4} - 10^{-3}$ in the MPS model, will be roughly equivalent to the dimensional artificial viscosity value $\alpha_0 c_0 h$ in the range of 0.027 – 0.23 in the SPH model.

From Fig.15, it can be seen that the best match result with the experiment data is achieved when α is between $1.08\text{x}10^{-1}$ and $3\text{x}10^{-1}$ for SPH, and $\upsilon_0 = 10^{-3}$ for MPS. For low viscosity value that represents the fluid that was used in the experiment, the numerical simulation results are slightly different from experiment data. It is due to circumstances in which the experiment and measurement were conducted. One of them is the fact that it is almost impossible to lift the wall instantly on the experiment (Lee *et al.*, 2011). Another thing that contribute to the aforementioned difference between the experiment result and the classical SPH model is that due to the occurence of the gap between the fluid continuum and the wall. The gap caused the relationship between the fluid and the boundary particles in a tangential direction to disappear, implicitly imitating a free-slip condition in classical SPH model.

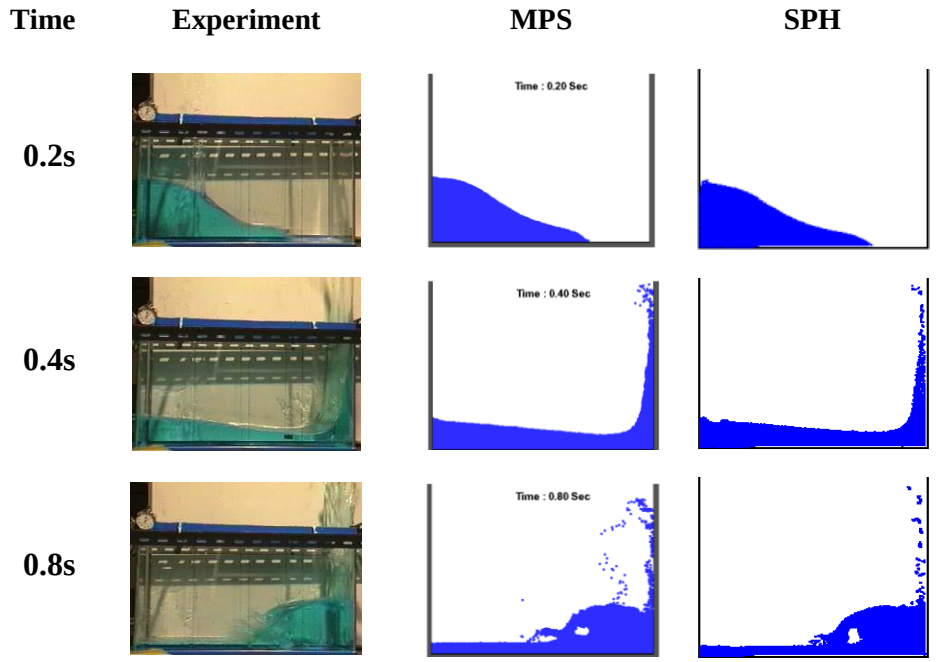

Figure 16: Dam break case snapshots comparison for MPS with and $\upsilon_0 = 10^{-6}$ and SPH with $\alpha = 1.08x10^{-5}$

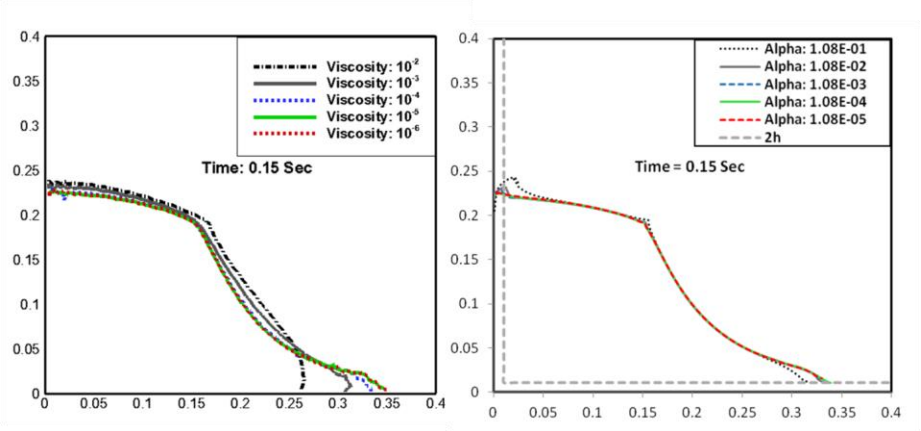

Figure 17: Dam break case instantaneous free surface MPS for various kinematic viscosity values υ_0 (left) and SPH for various artificial viscosity coefficient values α_0 (right)

On snapshot comparison for various time frames in Fig. 16**,** we can observe a good agreement between both models at low viscosity value, with the experiment result. On the

instantaneous free surface representation of the MPS and SPH simulation in Fig. 17**,** the overall free surface behaviour between the two methods is different. While the edges of the MPS free surface tends to curve more with higher viscosity, the edges of the SPH free surface tends to sharpen with higher viscosity value. Furthermore, higher sensitivity to viscosity value is once more observed in the MPS model.

The free surface representation of the SPH simulation in Fig. 17, shows the disturbance caused by the boundary particles on the left and bottom wall, where particles along the boundary seem to have been pushed further away from the wall than it is supposed to, resulting an unphysical gap to emerge between the fluids and the wall. Although it can not be seen clearly, the gap between the fluid particles and the wall particles also exists in Fig. 16**.** The gap typically has a width of r_e, which corresponds to the effective range where the dynamic boundary condition of the SPH begins to exert pressure to the incoming fluid particle.

The gap on the classical SPH model is caused by the velocity discontinuity between the wall particles and the fluid particles. Due to the continuity equation (Equation (21)) and the equation of state (Equation (29), the discontinuity in velocity will result in exaggerated pressure. Because of this feature on the classical SPH model, one can not simply take the boundary particle's pressure value to measure the fluid pressure on the point of interest. A dummy point that does not interact with any particles and located at a distance r_e from any wall particle need to be introduced if one wants to measure a fluid pressure near the wall.

3.2. Harmonic Sloshing Tank Case

A sloshing case is adopted to compare qualitatively the pressure profile of fluid impacting a wall. A 2D sloshing tank with dimension as shown in Fig. 18**.** The tank, that is represented by boundary particles, is moved in the lateral horizontal direction with a movement prescribed as, $X_H = 0.05\ sin\left(\frac{2\pi}{1.3}t\right)$.

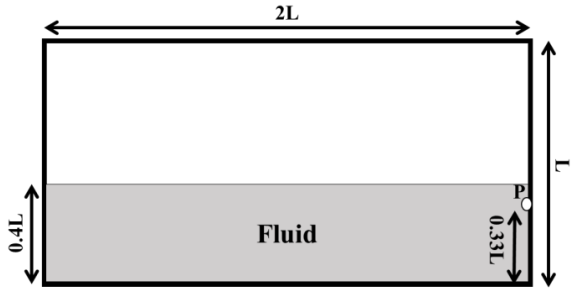

Figure 18: Harmonic sloshing tank case setup

The tank is moved with an amplitude of A = 0.05 m and a period of T = 1.3 sec. The pressure profile is calculated at point P as shown in Fig. 18 above. An impact pressure that will have the same period as the tank movement is expected. However, an exact match of the impact pressure magnitude with the experiment is almost impossible, since the obtained impact pressure from the experiment itself is not completely reproducible (Lee *et al.*, 2011). The peak amplitudes also depend on sensor size and resolution. Therefore, the impact pressure comparison will only be done in term of its period and profile tendency over time.

The simulation time T = 12 sec, L = 0.30 m water density ρ_o = 1000 kg/m^3, gravitational acceleration = 9.81 m/s^2, and initial distance between two neighboring particle dp_o=

0.0025 m are used. The total number of the fluid particle is 11233 particles. The artificial viscosity coefficient α_o=0.1 is selected based on the best-matched case in Fig. 15 and reference speed of sound c_o = 50 m/s are used in the SPH model and has successfully kept the density variation below 1%. The kinematic viscosity υ_o=10^{-6} is used for the MPS model. It is anticipated that the differences of the results in the range of υ_o=10^{-4} - 10^{-6} should be minimal judging from the previous case. Other parameters are taken to be the same with the dam break case setup, shown in Table 1.

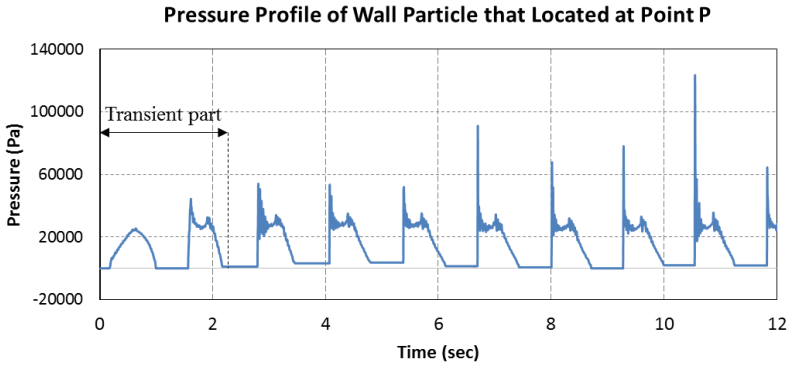

Figure 19: Sloshing case pressure profile of a wall particle that is located at point P on the SPH model

The raw pressure profile of a wall particle that is located at point P in the SPH model can be seen in the Fig. 19. From this figure, we can further confirm the presence of exaggerated pressure exerted by the wall particles. On the same figure, we can also observe the transient part that will be removed later for the comparative study.

In the DualSPHysics v3.1, there is an option where the hydrodynamics pressure at arbitrary points can be calculated using interpolation from the surrounding fluid particles. Therefore, we can still calculate the hydrodynamic pressure without using the pressure

from the wall particles. However, There is no option for where the user can make a moving observation point, which is needed for the sloshing case study. Due to the presence of the gap between the fluid and the wall, the moving observation point also need to be located at least at a distance of r_e from the wall at all time. By using the pressure profile obtained from a large number of static observation points, we can simulate a moving observation point. This procedure was done by extracting the pressure value from a particular static observation point with a same coordinate as the point P, as point P moved along with the tank at each time step.

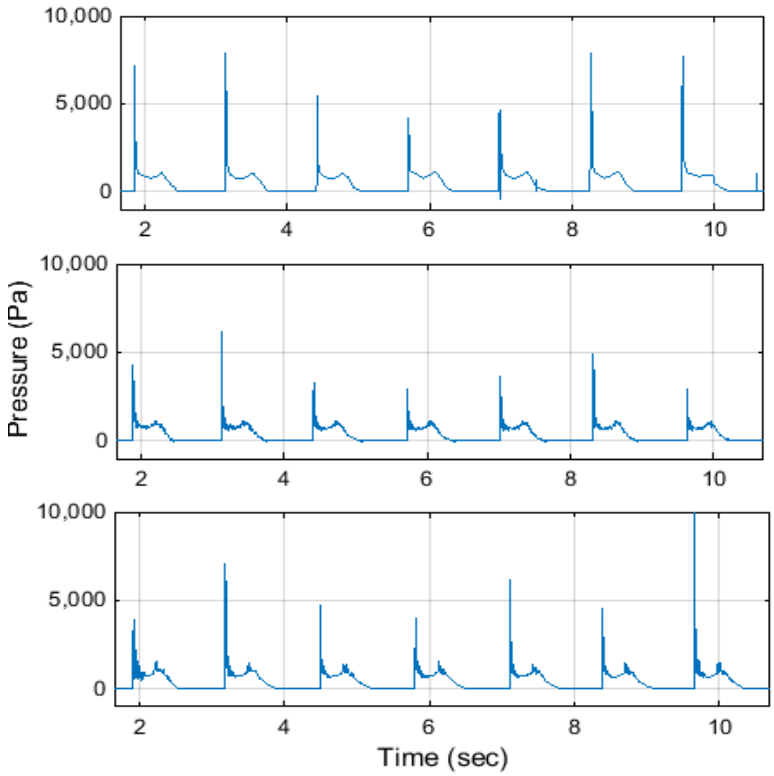

Figure 20: Sloshing case pressure profiles comparison, from top to bottom experiment, MPS, SPH

The impact pressure at point P over time can be seen in Fig. 20, while the free surface comparison between the experiment, SPH model, and MPS model can be seen in Fig. 21. The pressure profile of the SPH model was obtained by using the aforementioned method. The transient part of the simulation has been removed from the plot. The t=0 on the experiment does not mark the time when the experiment began. Hence, the pressure profile of the MPS and the SPH model was shifted so that their first impact pressure coincides with the first impact pressure on the experiment. The free surface comparison in Fig. 21 was also obtained after the removal of the transient part.

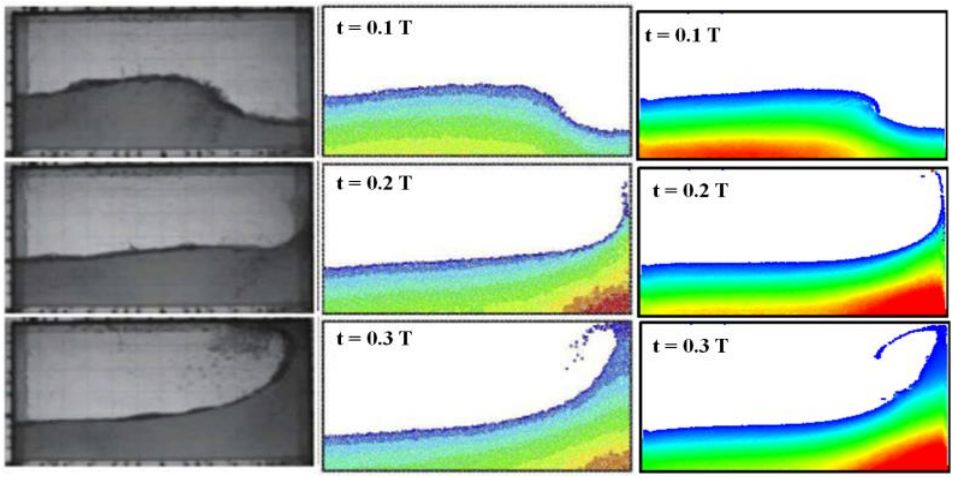

Figure 21: Sloshing case free surface comparison between the experiment (Left), MPS (Middle), and SPH (Right). Colors represent normalized pressure.

Recently, the present MPS method has been extended to handle multi-liquid simulations and the corresponding multi-interface sloshing problem. The improvements include the surface tension model, buoyancy-correction model, interface searching method, and also interface boundary conditions. The model has successfully reproduced the internal free surface motions that were observed on the experiment. More detailed explanation of the

MPS application on multi-liquid simulation, including sloshing simulation with multi liquid layers can be found in Kim et.al (2014).

3.3. Computation Efficiency

For computation time comparison, three different numbers of particles are used to simulate sloshing and dam break case. DualSPHysics v.3.1 was run in CPU mode for better comparison. However, please note that DualSPHysics v.3.1 utilize parallel algorithm in its code while the in-house MPS program does not. To better understand the effect of computational effort on accuracy in both methods, pressure profile comparison is done for the dam break case. The dam break simulation setup is similar to the one used in Fig. 18, but instead of using 4xL as the tank length, 2.5xL is used to save time. L = 0.4 m is used, and point P at $(x, z) = (\, 2.5\, L, 0.25\, L)$ is used as observation point for pressure profile comparison. The artificial viscosity coefficient $\alpha = 0.01$, and reference speed of sound $c_o = 55\, m/s$ are used in the comparison of computation effort effects on accuracy. The dam break case is simulated for 3 sec, and the sloshing case is simulated for 6.5 sec. The average computation time is plotted in Fig. 22, while the effect of computation effort on accuracy can be seen in Fig. 23.

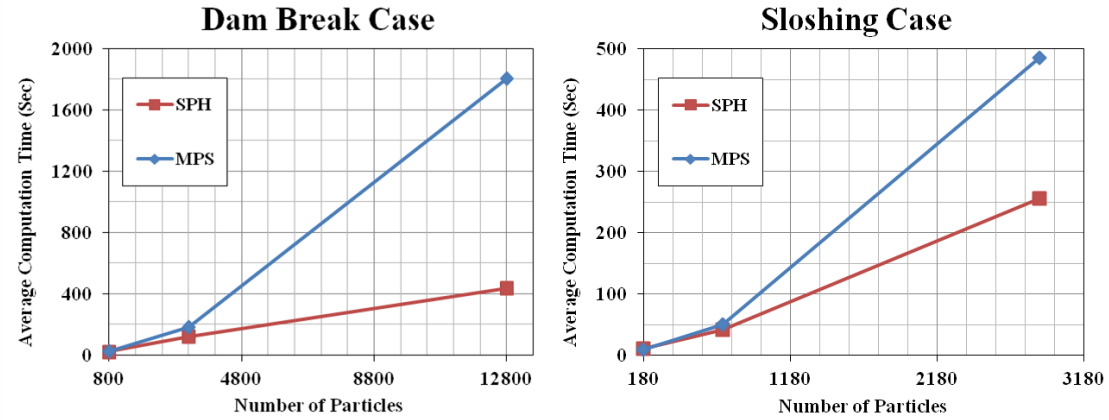

Figure 22: Computation time comparison between the MPS and SPH model for various number of particles

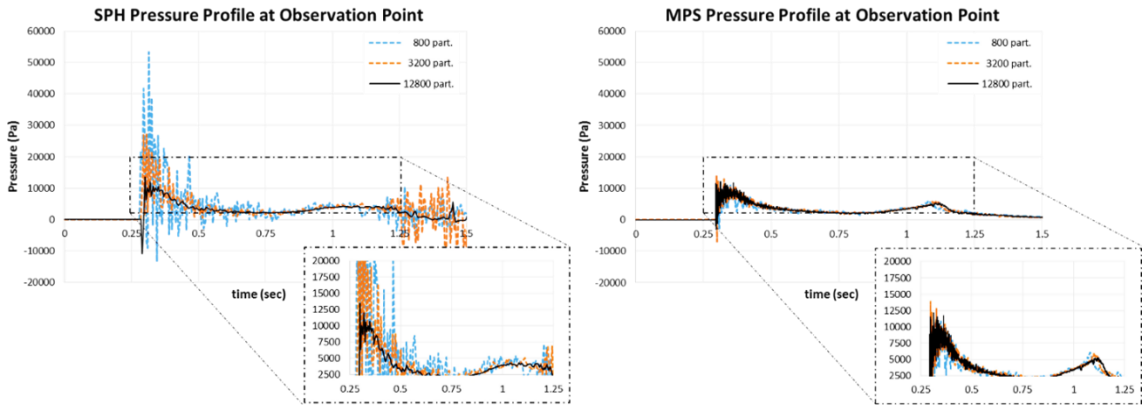

Figure 23: Dam break case pressure profile at observation point, with various number of particles

From Fig. 22**,** we can see that SPH solver program is significantly less time consuming and more efficient for large number of particles compared to the MPS solver program. The difference mainly comes from the need of solving Poisson equation for pressure calculation in MPS, and also the parallel algorithm utilized by the SPH solver. However, as mentioned before, the SPH method needed a cumbersome post-processing to obtain a

reasonable pressure profile. Furthermore, without using Poisson equation for pressure calculation, its accuracy may not be warranted.

As can be seen in Fig. 23, MPS need a smaller number of particles to achieve the same result as the SPH. This means that MPS can save computation time by using coarser discretization than SPH, for similar accuracy. On the same figure, one can also see that MPS is much less sensitive to the number of particles that is used. Therefore, the computational efficiency of SPH compared to MPS should not be too much emphasized.

4. IMPROVEMENTS ON THE SPHYSICS BOUNDARY CONDITION

The scope of the SPH improvements in the present study is focused on the implementation of newly developed boundary condition by Adami, et.al. (2012) and the adoption of the MPS collision model by Kim, et.al. (2010) to the SPHysics program (Gomez-Gesteira *et al.*, 2012a and Gomez-Gesteira *et al.*, 2012b). The change of overall characteristics of the model is studied by repeating the test cases that are done in the previous chapter. An additional case of piston type wave maker is simulated after the improvements. The wave maker case are chosen because the kinematics of the case are dominated by the boundary treatments, which are the vocal point of present study.

4.1. Adami Boundary Condition and Collision Model

The algorithm of how the pressure of the wall particles is calculated by the dynamic boundary condition method can be seen in Appendix A. From the algorithm, we can see that the pressure of the wall and fluid particles are not directly related. On the wall particles, the error introduced in the equation of state will further add to the overall error from the continuity equation. On the MPS method, this is avoided by the use of the Poisson pressure equation that relates the pressure of the wall and fluid particles directly.

Adami *et.al.* (2012), derived the relation in which the pressure of wall particles can be calculated from the pressure of the fluid particles. A force balance between a wall and a fluid particle gives

$$\frac{D\vec{u}_f}{Dt} = -\frac{1}{\rho_f}\nabla P_f + \vec{g} = \vec{a}_w \quad (56)$$

Where subscript *f* and *w* denotes fluid and wall particle respectively, a_w is the prescribed wall particle's acceleration, and $\vec{g}$ is the gravitational acceleration. Note that this equation does not include the viscosity term. Therefore, viscosity term calculation between the fluid particle and the wall particle need to be turned off for best result. Integrating the balanced force equation along the centerline of the two particles, we find

$$\int \nabla P.\overrightarrow{dl} = \rho_f \int (\vec{g} - \vec{a}_w).\overrightarrow{dl} \quad (57)$$

$$P_w = P_f + \rho_f(\vec{g} - \vec{a}_w).\vec{r}_{wf} \quad (58)$$

Where $\overrightarrow{dl}$ is the vectorial length element along the centerline of the two particles, and $\vec{r}_{wf}$ is the position vector between the two particles. Since a wall particles interact with several fluid particles, the discretized SPH interpolation form (Equation (4)) need to be utilized to the right-hand side of Equation (58). This gives

$$P_w = \frac{\sum_f \frac{m_j}{\rho_j} P_j w_{wj} + (\vec{g} - \vec{a}_w).\sum_f m_j \vec{r}_{wj} w_{wj}}{\sum_f \frac{m_j}{\rho_j} w_{wj}} \quad (59)$$

From the obtained pressure, density of the wall particle can be calculated using the equation of state relation

$$\rho_w = \rho_0 \left[\left(\frac{P_w}{\mathrm{B}}\right) + 1\right]^{1/\gamma} \quad (60)$$

The Equation (59) above is slightly different from the wall pressure equation presented in Adami et.al. (2012). The difference comes from the use of m_j/ρ_j term inside the summation in the Equation (59), to maintain consistency of the discretized SPH interpolation form that is used throughout the SPHysics source code. Besides the difference mentioned above, there are several other slight differences between the SPHysics and Adami *et.al.* (2012), such as in the discretized continuity and momentum formulation. Therefore, different behavior and characteristic between the two formulations might present, and the use of Equation (59) in the SPHysics program remain an interesting and challenging topic to study.

A preliminary study of a hydrostatic tank suggested that the Equation (59) alone not suffice to keep the fluid particle from penetrating the solid wall particles, especially on the sharp corner of the wall. The use of collision model such as explained in the subsection 2.1 is proved to be useful to overcome this problem, as can be seen in Fig. 24.

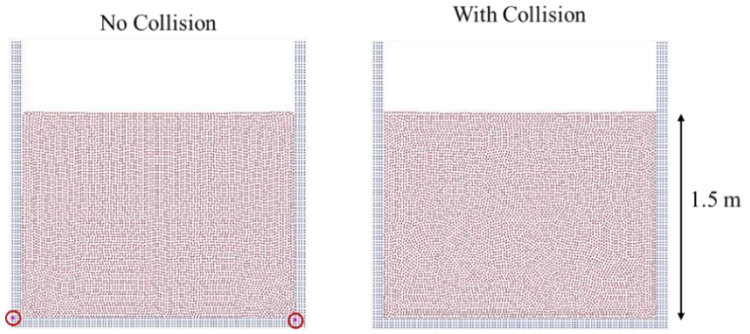

Figure 24: Fluid particles penetrating the wall particles in absence of collision model. The escaped fluid particles are marked by red circles.

We can see in the Fig. 25 that without the use of collision model, the maximum pressure fluctuation due to the propagation of the acoustic wave is alternating between the two corners of the wall. On the other hand, when collision model is implemented, the maximum pressure fluctuation is contained only in the vertical direction, a result that is expected from the hydrostatic tank case. The pressure at the mid-bottom wall of the tank can be seen in Fig. 26, and it shows that the collision model only slightly affect the phase and the maxima-minima value. Note that the presented pressure value was obtained directly from the wall particle's pressure value, which was impossible to be done when dynamic boundary particle method is used.

After the implementation of Adami boundary condition and the collision model in the SPHysics program, the overall algorithm can be seen in Appendix B. The downside of the use of the proposed algorithm is that the wall pressure need to be calculated after the calculation of the fluid pressure. This does not significantly affect the computation time when the computation is done in a series manner. However when parallel computing is utilized; the wall pressure calculation will become a bottleneck. Furthermore, the calculation of the collision model also increases the computation time.

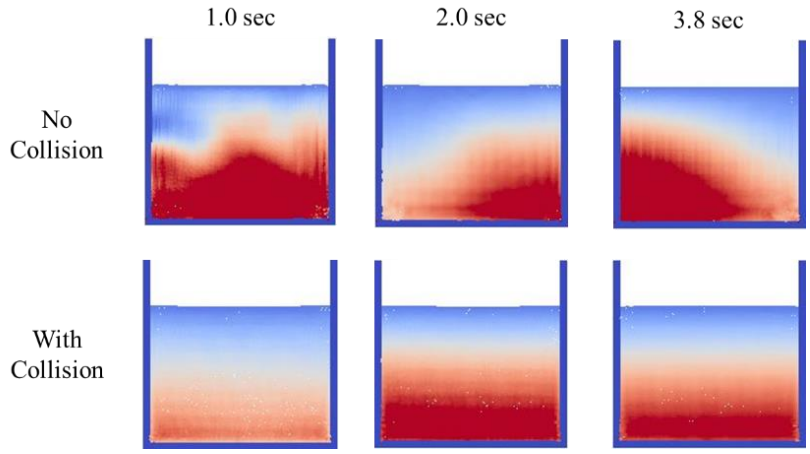

Figure 25: Fluctuation of maxima and minima pressure distribution on hydrostatic tank test case

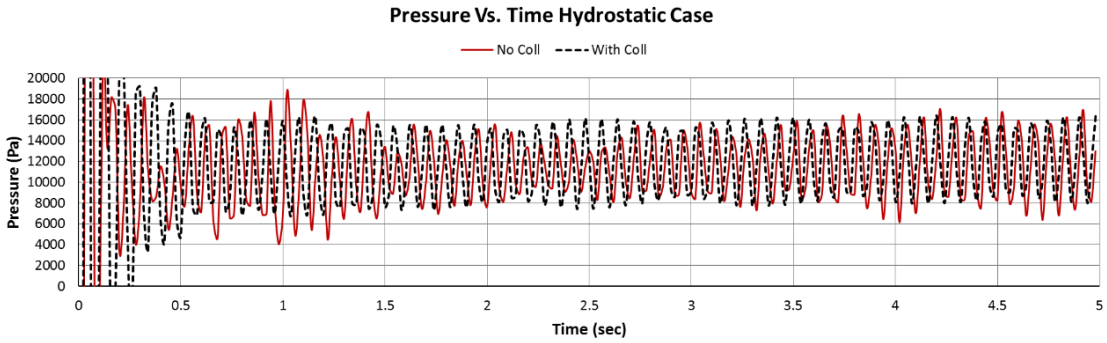

Figure 26: Pressure fluctuation on the mid-bottom wall of the hydrostatic tank

4.2. Dam Break Case

A dam break case with the same setup as in subsection 3.1 is used to investigate the characteristic and general behavior of the newly adopted Adami boundary condition and the collision model. Fig. 27 below shows the free surface representation of the SPH model with Adami boundary condition and collision model, classic SPH model with dynamic boundary condition, and the experiment result. The artificial viscosity coefficient that is

used is $\alpha \leq O(10^{-2})$, and the collision coefficients $a = 0.80$ and $b = 0.2$ is used with the Adami B.C.

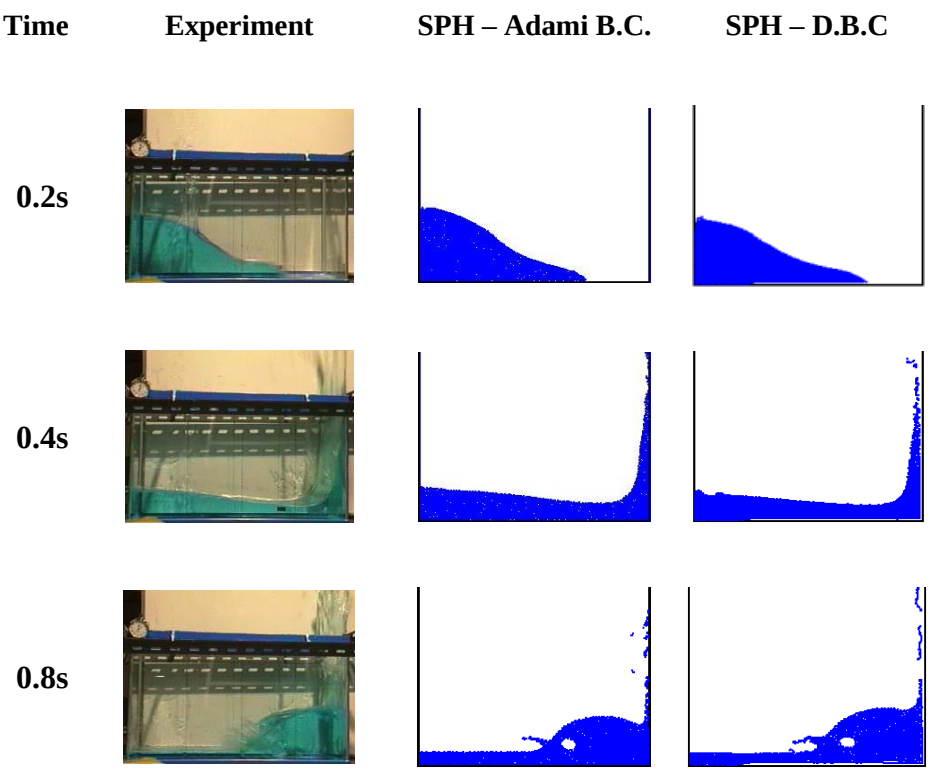

Figure 27: Dam break case free surface comparison between the classical SPH and the newly implemented B.C., for low viscosity value

From Fig. 27 above, we can see that the gap between the wall and fluid particles had successfully removed when Adami B.C is used while still maintaining its conformity to the experiment result. The comparison between the particles position near the boundary of both boundary condition can be seen in Fig. 28.

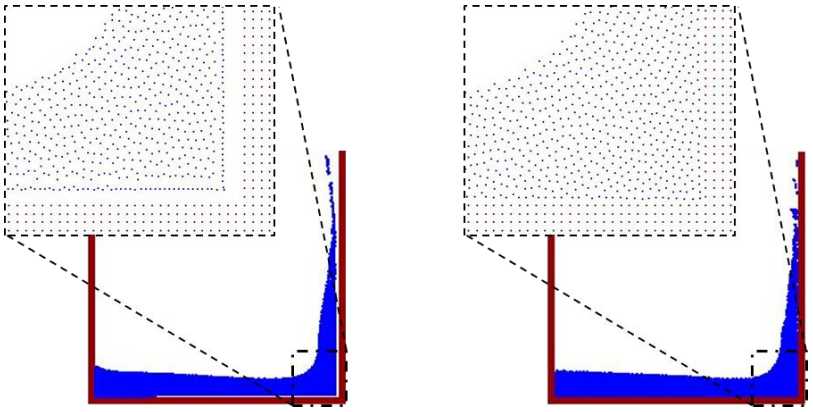

Figure 28: Particles position near the boundary of the SPHysics model using D.B.C. (Left) and Adami B.C. (Right)

It can be seen in Fig. 28 that by using the Adami B.C., the fluid particles on the right wall is moving up along the wall without any disturbance, a characteristic that is not presence on the SPH with a dynamic boundary condition. However, if the shear interaction from the viscosity term between the wall and fluid particles in the Adami B.C. is not removed, the fluid particles will experience disturbance as they move along the wall. This disturbance can be seen in Fig. 29 below. This is due to the absence of the viscosity effect in the force balance formulation (Equation (56)).

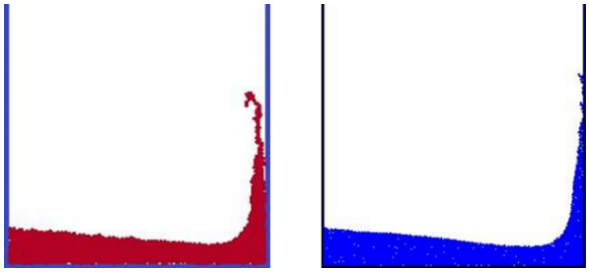

Figure 29: Comparison of Adami B.C. with the viscous interaction on the wall activated (left), and removed (right)

To investigate the effect of viscosity on the SPHysics program with Adami B.C., several artificial viscosity value α is used to study the kinematics of the model. The model parameters and the viscosity values are made identical with the one used in subsection 3.1. The collision coefficients $a = 0.80$ and $b = 0.2$ are used. These collision coefficients are chosen after several initial study shows that if not chosen properly, fluid particles can still penetrate wall particles, or in some other cases, fluid particle unphysically bounced off wall particles at high velocity. The resulting leading edge propagation and the free surface representation can be seen in Fig. 30.

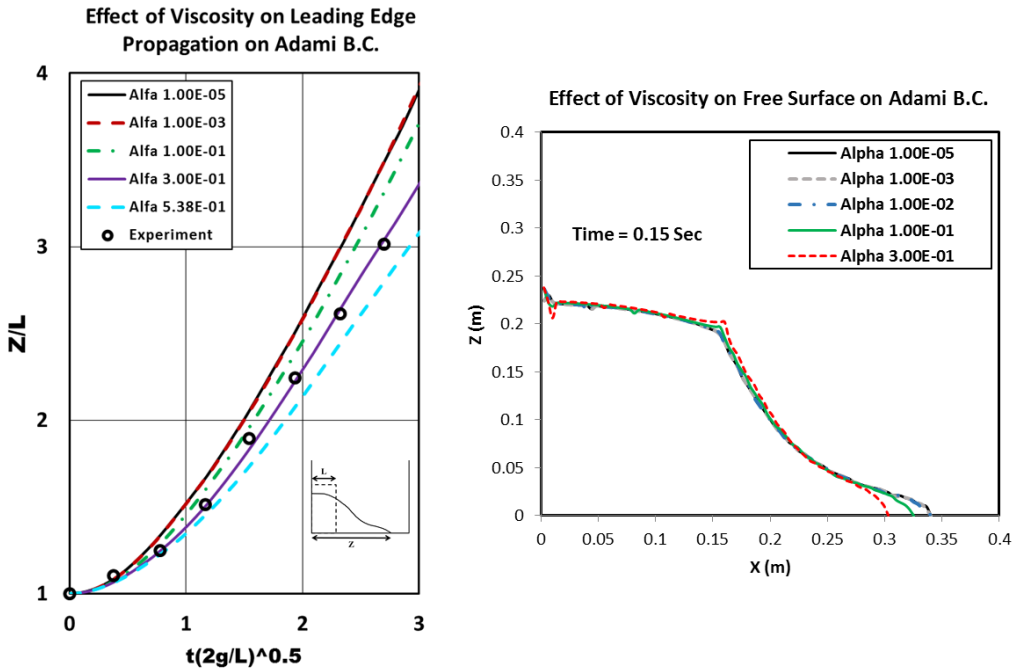

Figure 30: Viscosity effect on the dam break case kinematics, after the Adami B.C. and collision model implementation

Fig. 30 shows that the kinematics are almost unaffected by the choice of α, when $\alpha \leq O(10^{-2})$, thus can be considered as inviscid inside aforementioned range of α. The

experiment result almost completely coincides with $\alpha = 0.3$, instead of located within certain α band such as observed on the SPH model with D.B.C. To further investigates the change in the characteristic of the SPH model due to the Adami B.C. and the collision model, several model parameter combinations are modeled, and plotted side by side with its counterpart classical SPH model. The results can be seen in Fig. 31 below, where the numbers denote the artificial viscosity coefficients, "old" marked the D.B.C model, "new" marked the Adami B.C. model, the first two digits after "Coll" denote the a coefficient of the collision model, and the last two digits after "Coll" denote the b coefficient of the collision model.

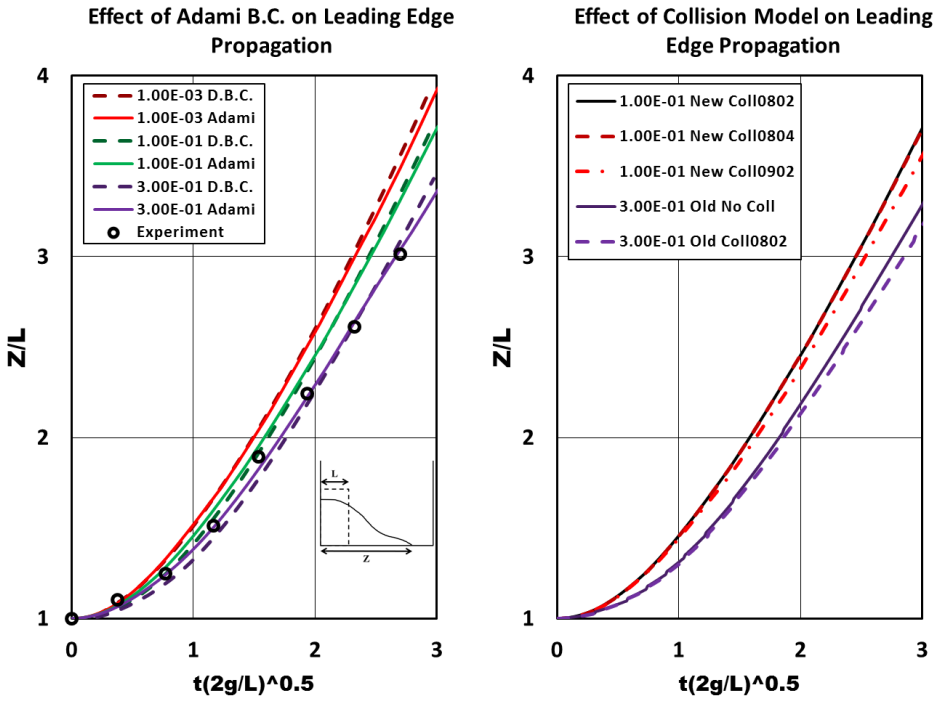

Figure 31: The effect of Adami B.C. and the collision model to the kinematics of the dam break case

On the Fig. 31 above, we can deduce the leading edge velocity from the gradient of the leading edge propagation graph. From the left figure, it is observed that in overall the Adami B.C. cases reached their maximum velocity faster than the D.B.C cases. However, the maximum velocity of the Adami B.C is observed to be slower than the D.B.C cases. This is because the D.B.C need to wait for the gap to emerge to cancel the viscous shear effect between the wall and the fluid particles. This has caused experiment result to fall within certain α band on the D.B.C case. The behavior as mentioned above is less apparent in low viscosity value.

From the right figure of Fig. 31, we can deduce that the collision model slows the leading edge propagation, even when D.B.C. is used. This is due to the mechanism of the collision model itself that transfer momentum from one particle to another particle, thus mimic the effect of viscosity. Although similar, the collision model is, in fact, different from viscosity model, due to the fact that it only acts between two interacting particles, instead of acting as a continuum. From the same figure, we also observed that the choice of collision range coefficient a have a bigger role in affecting the kinematics then the choice of collision rate coefficient b. However, note that the study of the leading edge propagation does not involve a high-velocity impact, a condition where collision rate coefficient might play a bigger role in the result.

Several collision coefficients combinations are modeled to investigate the effects of the collision model to SPHysics dynamics. These cases can be seen in Table 3. The tank is slightly modified to safe computation time. Instead of using 4xL as the tank length, 2.5xL

is used. L = 0.4 m, artificial viscosity coefficient $\alpha = 0.01$, reference speed of sound $c_o = 55\, m/s$, and 3200 particles are used. Point P at $(x, z) = (2.5\, L, 0.25\, L)$ is used as an observation point for pressure profile comparison. The resulting pressure on point P can be seen in Fig. 32.

Table 3: Case definition for collision coefficient sensitivity study

Name	**Boundary Condition**	***a***	***b***
Case 1	D.B.C.	Non	Non
Case 2	Adami B.C	0.80	0.20
Case 3	Adami B.C	0.80	0.35
Case 4	Adami B.C	0.92	0.20
Case 5	Adami B.C	0.92	0.35

From Fig. 32 we can see that, in general, a higher collision rate coefficient b reduced the minimum pressure on the initial impact, and a lower collision rate will shift the maxima impact pressure slightly to the right. From the figure, we can also deduce that the choice of $a = 0.80 - 0.92$ and $b = 0.20$ are reasonable since they do not change the overall pressure characteristic drastically. However, the exact number of the coefficient should be chosen on a case by case basis for best result.

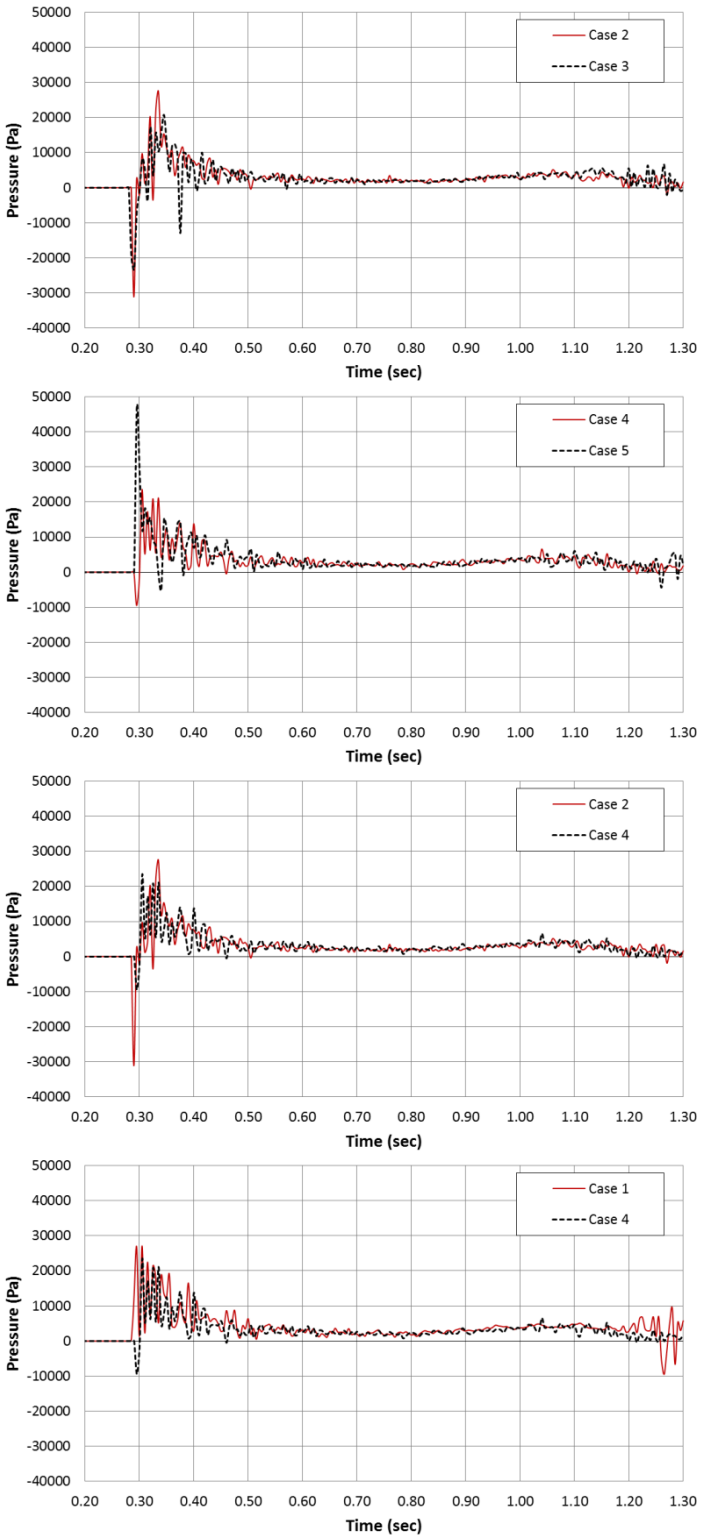

Figure 32: The effect of the choice of coefficient ratio to the dam break case dynamics

It is observed that the collision model does not give any improvement in the stability of the pressure variation. This is quite different from what was observed on the MPS, where the collision model improves the stability of the model (Lee *et al.*, 2011). Nevertheless, the collision model is needed in the application of Adami B.C. in the SPHysics to ensure that no fluid particles can penetrate the wall particles and to overcome high pressure fluctuation on the sharp corners.

4.3. Harmonic Sloshing Tank Case

A sloshing case with the same setting as the one in subsection 3.2 is modeled using the SPHysics with Adami B.C. Collision ratio $a = 0.92$ and $b = 0.20$ are used. After the implementation of the Adami B.C., this particular case is interesting to study since it involve a prescribed position, velocity, and acceleration of the wall particles, both in perpendicular and tangential direction from the fluid continuum.

During the preliminary study, it was found that the fluid particles tend to stick to the upper wall of the tank, as can be seen in Fig. 33. This is due to the negative relative velocity between the upper wall and the splashed fluid particles. This then caused the density of the fluid to significantly droped, resulting a negative pressure on the fluid traveling along the upper wall. This unphysical behaviour was also related to the fact that the viscous interaction between the wall and fluid particles had been removed in order to compensate for the absence of the viscous force on the Equation (56). One way to avoid this problem is to introduce higher collision rate and larger collision activation range to the upper wall only, thus making the transfer of momentum from the collision model to dominate the

dynamics of the particles interacting with the upper wall. For this case, $a = 1$ and $b = 0.40$ is used on the proximity of upper wall particles. However, this approach is still not addressing the root of the problem, which is the boundary condition formulation itself.

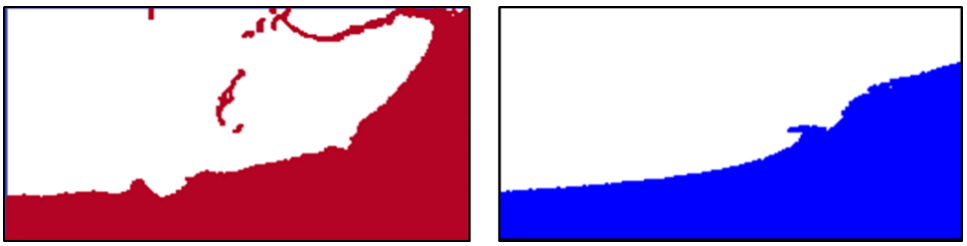

Figure 33: Wall particles stick to the upper wall without any special treatment (left), and wall particles not sticking anymore after special treatment on the upper wall (right)

The free surface comparison between the experiment, SPH model with Adami B.C.m and SPH model with D.B.C. can be seen in Fig. 34. The observed and the simulated free surface profile of the SPH model with Adami B.C. show good agreement. The free surface profile between the two SPH model also shows good agreement, with only minor differences near the boundaries. On the bottom boundary of the SPH model with Adami B.C., the pressure profile is slightly disturbed. This is mainly due to the absence of the tangential viscous shear stress between the wall and fluid particles, hence as the wall moves back and forth, collision model become more dominant in the tangential momentum transfer.

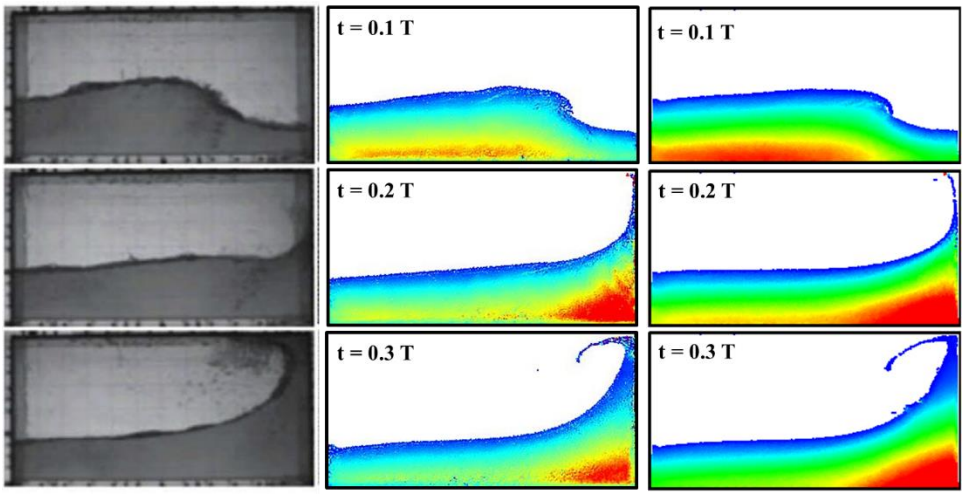

Figure 34: Sloshing case free surface comparison between the experiment (Left), SPH with Adami B.C. (Middle), and SPH with D.B.C. (Right). Colors represent normalized pressure.

The impact pressure at point P as defined in sub section 3.2, can be seen in Fig. 18. Once again, a good agreement between the model and the experiment results can be obtained. Note that unlike in the SPH model with D.B.C., this pressure profile were obtained directly from the wall particle. The impact period, measured from peak to peak of the pressure profile, is measured to be 1.3 sec, which is a good match with the movement period of the tank. The characteristic of the pressure profile also shows a good agreement, where both experiment and model result from SPH with Adami B.C. shows the occurrence of one high pressure peak followed by lower pressure peak in each cycle. It can be concluded that, although having difficulties in dealing with dynamics in the tangential direction, the Adami B.C., combined with the collision model has successfully captured all the essential features of the harmonic sloshing tank case.

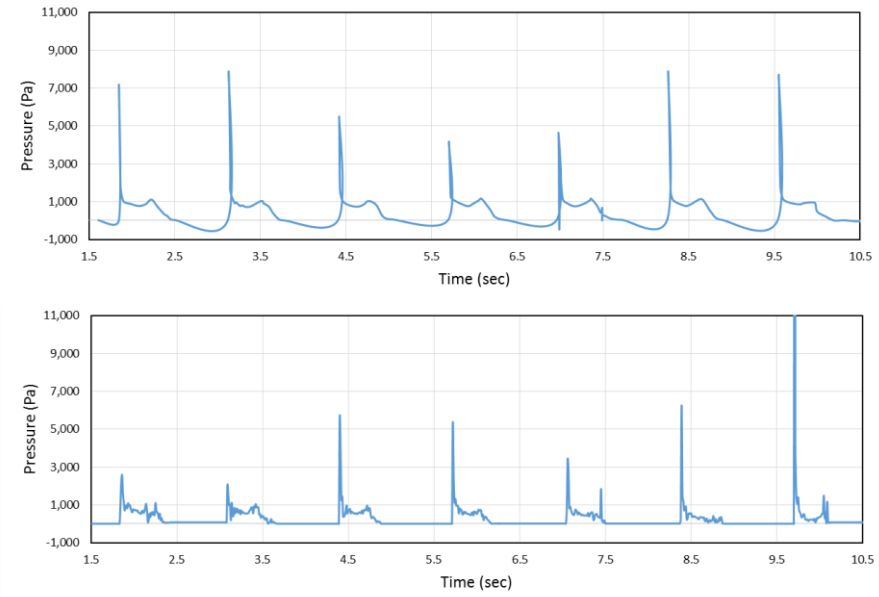

Figure 35: Sloshing case pressure profile comparison between experiment (top), and SPH with Adami B.C. (bottom)

4.4. Wave Maker Case

A wave maker case is tested using the newly implemented boundary condition and collision model. Far field boundary treatment methods to attenuate the effect of the reflecting waves in a wave maker simulation are presented in many studies. Most of these studies, such was done by Omdivar (2010) and Molteni et.al. (2012), utilize a mathematical and numerical manipulation to damp the kinematics and dynamics of the SPH particles far away from the wave maker. In the present study, a physical damper in the form of sponge layer is used to avoid any additional numerical manipulation. This approach is used because it resembles the porous wall that is typically used as wave damper in the physical wave tank. The particles configuration of the sponge layer can be seen in Fig. 36 below.

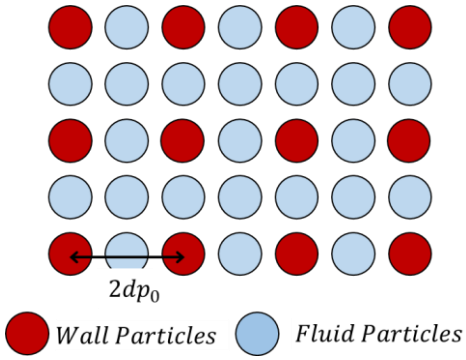

Figure 36: Initial particle configuration of the sponge layer

A piston type wave maker is used and moved in the lateral horizontal direction with a prescribed movement of, $X_H = 0.08h\ sin\left(\frac{2\pi}{T}t\right)$. The case geometry can be seen in the Fig. 37 and Fig. 38. Where h is the water depth, and L_o is theoretical wavelength calculated using dispersion relation from linear potential wave theory. Two wave gauges were placed to measure the water elevation at a point at any given time.

Preliminary studies suggested that if artificial viscosity were too small, the particles movements became too unstable, and a variation in the free surface due to the wave maker movements cannot be seen clearly. The case setup for the wave maker case can be seen on Table 4.

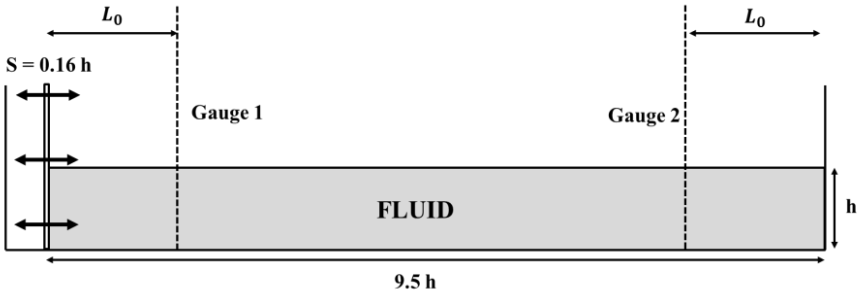

Figure 37: Wave maker with solid wall case setup

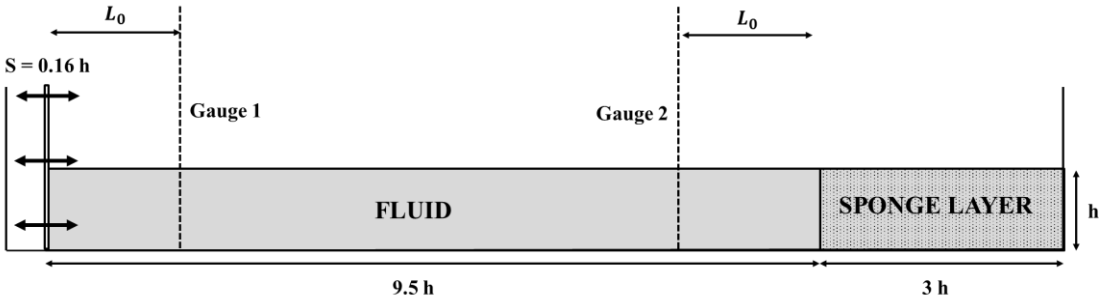

Figure 38: Wave maker with sponge layer case setup

Table 4: Wave maker case setup

Case setup	
Simulation time	60 sec
H	1 m
ρ_o	1000 kg/m3
G	9.81 m/sec^2
dp_o	0.02 m
Number fluid of particles	23650 & 29275 particles
α	0.003
Collision coefficient a	0.80
Collision coefficient b	0.20
c_0	150 m/sec
T	1 sec
L_0	1.56 m

Using linear potential theory, Dean & Dalrymple (1991) showed that the wave height to stroke length ratio for piston type wave maker can be written as

$$\frac{H}{S} = \frac{2(\cosh 2kh - 1)}{\sinh 2kh + 2kh} \quad (61)$$

Where H is the wave height in positions that is relatively far from the wave maker, S is the stroke of the wave maker, and $k = 2\pi/L$. From the given parameters, the ratio for

this particular case is $H/S = 1.9885$. Using the wave height to stroke ratio, the wave height due to wave maker alone can be estimated as $H \approx 0.3182\, m$. The Equation (61) and the dispersion relation are derived under the assumption of a totally incompressible and inviscid fluid, which both are not true in the SPH model. However, it can still give a starting point for the prediction of the numerical model results.

The wave height of the wave maker case without the sponge layer is expected to be larger than the hypothesized wave height. This is due to wave reflected back to the domain after it hit the solid vertical wall. Dean & Dalrymple (1991) formulated that when waves hit a solid vertical wall, the fully developed wave height should be twice the incoming wave height. Combined with the hypothesized wave height to stroke ratio, this gives us rough estimates of the wave heights of $H \approx 0.6364\, m$ for the wave maker case without the sponge layer. The measured water elevations on both wave gauge are presented in Fig. 39 below.

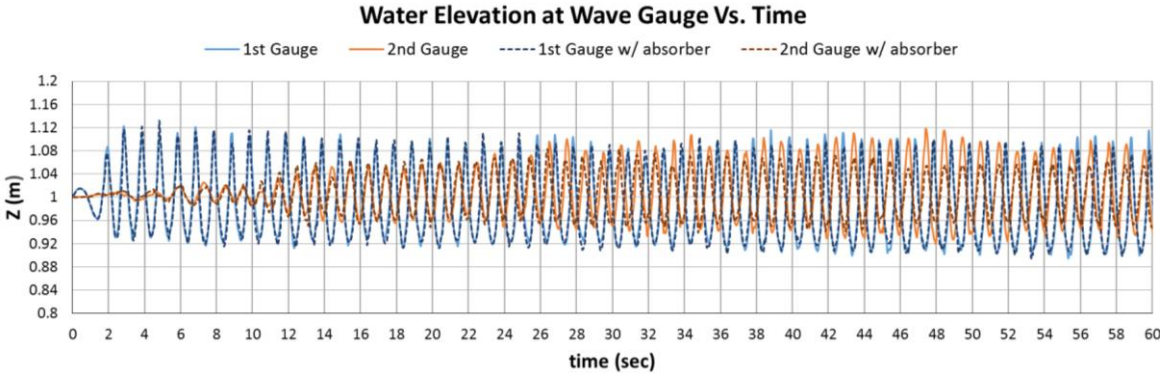

Figure 39: Water elevation at wave gauges for wave maker case with sponge layer, and wave maker case without sponge layer

From the Fig. 39, we can observe how the wave amplitude developed over time. The solid line represents the wave maker case without the sponge layer (Fig. 37) while the dashed line represents the wave maker case the sponge layer (Fig. 38). The wave elevation at the second wave gauge of the wave maker case without the use of sponge layer can be seen to have three distinct stages. The first stage is between 0 – 12 sec, in which the wave train is yet to arrive at the second wave gauge. The second stage is from 12 – 26 sec, in which the wave height seems to have stabilized under a certain period. The third stage, marked by a noticeable increase in wave height after 26 sec.

The third stage, is not present in the case where the sponge layer is used, where after 12 sec, the wave height does not show any noticeable variation. Therefore, it can be deduced that the rise in wave height at the second wave gauge of the case without the sponge layer, was due to the reflected wave that reached the second gauge a few moments after the initial propagating wave reached that point. It also indicates that the propagating wave was successfully absorbed by the sponge layer in the case when the sponge layer is used. However, the rise of the wave height does not appear at the 1st gauge at all, even for the case without the sponge layer. The aforementioned problem will be discussed later, with the help of wave statistics that can be seen in Table 5 below. The numbers on Table 5 are obtained by using zero up crossing method. We can see from Table 5 that the wave period is consistent with the prescribed wave maker oscillation period, which is 1 sec. On the same table, the wave height difference between the case with and without sponge layer at the 2nd wave gauge can be clearly seen. The ratio of the maximum wave height of the case without sponge layer to the case with sponge layer is ≈ 1.488, a number that is smaller

than the theoretical ratio, which supposed to be 2. Two possibilities can explain this phenomena, the first is that there is an unsuspected absorption on the vertical wall boundary and the second is that energy is dissipated inside the fluid continuum.

Table 5: Wave statistics measured at the wave gauges

1st Gauge			**1st Gauge w/ absorber**			**2nd Gauge**			**2nd Gauge w/ absorber**		
H_{max}	0.212	m	H_{max}	0.201	m	H_{max}	0.198	M	H_{max}	0.133	m
T_{max}	1.001	sec	T_{max}	1.001	sec	T_{max}	1.001	Sec	T_{max}	1.000	sec
H_{mean}	0.184	m	H_{mean}	0.182	m	H_{mean}	0.121	M	H_{mean}	0.094	m
T_{mean}	1.002	sec	T_{mean}	1.002	sec	T_{mean}	1.004	Sec	T_{mean}	1.002	sec
$H_{1/3}$	0.199	m	$H_{1/3}$	0.194	m	$H_{1/3}$	0.169	M	$H_{1/3}$	0.120	m
$T_{1/3}$	1.001	sec	$T_{1/3}$	1.000	sec	$T_{1/3}$	1.001	Sec	$T_{1/3}$	1.008	sec
$H_{1/10}$	0.208	m	$H_{1/10}$	0.199	m	$H_{1/10}$	0.183	M	$H_{1/10}$	0.129	m
$T_{1/10}$	1.007	sec	$T_{1/10}$	1.000	sec	$T_{1/10}$	1.008	Sec	$T_{1/10}$	1.000	sec
$H_{1/20}$	0.211	m	$H_{1/20}$	0.200	m	$H_{1/20}$	0.192	M	$H_{1/20}$	0.131	m
$T_{1/20}$	1.001	sec	$T_{1/20}$	1.000	sec	$T_{1/20}$	1.014	Sec	$T_{1/20}$	0.987	sec

From the Table 5 and Fig. 39, it can be seen that the wave heights at 2nd gauge of the sponge layer case are significantly smaller than those that are observed at the 1st gauge. Since it was already deduced that the reflected wave was successfully absorbed by the sponge layer as if there is no solid boundary present, the height loss almost certainly does not have any correlation with the solid boundary. In other word, the energy dissipation inside the fluid continuum become the sole possibility that can explain the wave height loss.

The previous explanation can explain why the wave height at the first gauge in both cases is similar in magnitude. The energy from the reflected wave is already completely dissipated before it can reach the first gauge. The same explanation also caused the overall wave heights to be significantly smaller than the hypothesized wave height from Equation (61).

The loss of wave height in SPH had also been noted by other studies, namely by Vaughan (2005) and Palferene (2011). Vaughan covered in details on how the viscous energy become larger over time on solitary wave simulation, causing the solitary wave height to become smaller as it traveled away from the wave maker. From the aforementioned study, viscous dissipation can be assumed to be the underlying reason behind the loss of wave height in the current study as well. However, further study need to be done to confirm this, and to find a way to overcome this particular downside in the SPH wave making simulation.

At least two wave parameters ratio are needed to analyze the category of the waves according to Dean & Dalrymple (1991). These parameters ratio are $H/T^2 = 0.43 - 0.69\ ft/sec^2$ and $h/T^2 = 3.28 ft/sec^2$. From these ratios, the wave is categorized as deep water waves. The theoretical model based on potential theory that best fit the simulated waves is the Stokes 5th order theory as can be seen in Fig. 40 below. Stokes 5th order theory is a highly nonlinear wave theory, therefore even from the start, the linear wave maker theory cannot give a reliable estimation of the wave characteristics.

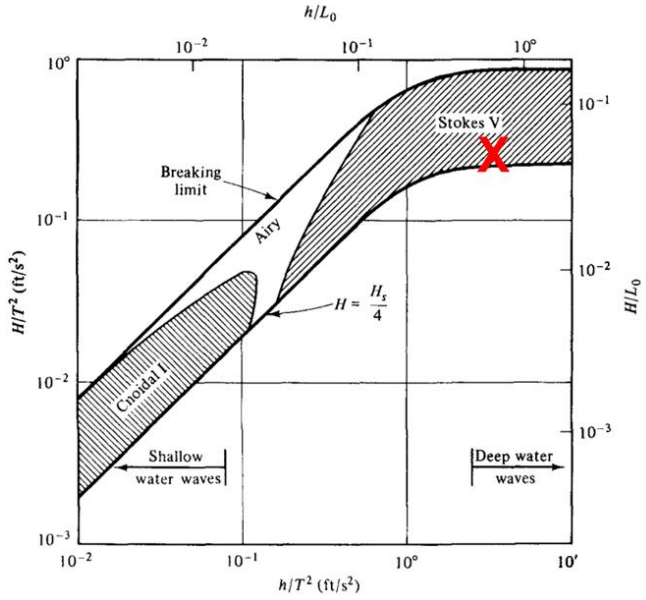

Figure 40: Wave theory category based on given wave characteristics. Red cross marks the simulated wave characterics

The instantaneous free surface profile of both cases can be seen in Fig. 41. To be able to see the free surface profile more clearly, fluctuation in the order of initial particle distance dp_0 was filtered out. On the case without the sponge layer, a standing wave can be clearly seen near the right boundary, marked by a node and envelope position that are always at the same points at any given time. However, the standing wave is only observed about one wavelength from the wall boundary. This result strengthens the previous argument that the reflected wave got dissipated after a certain distance from the boundary.

From the same figures, we can also see that in the case where the sponge layer is used, the phase angle near the right boundary is shifted to the right. This behavior is commonly observed when an open boundary is used.

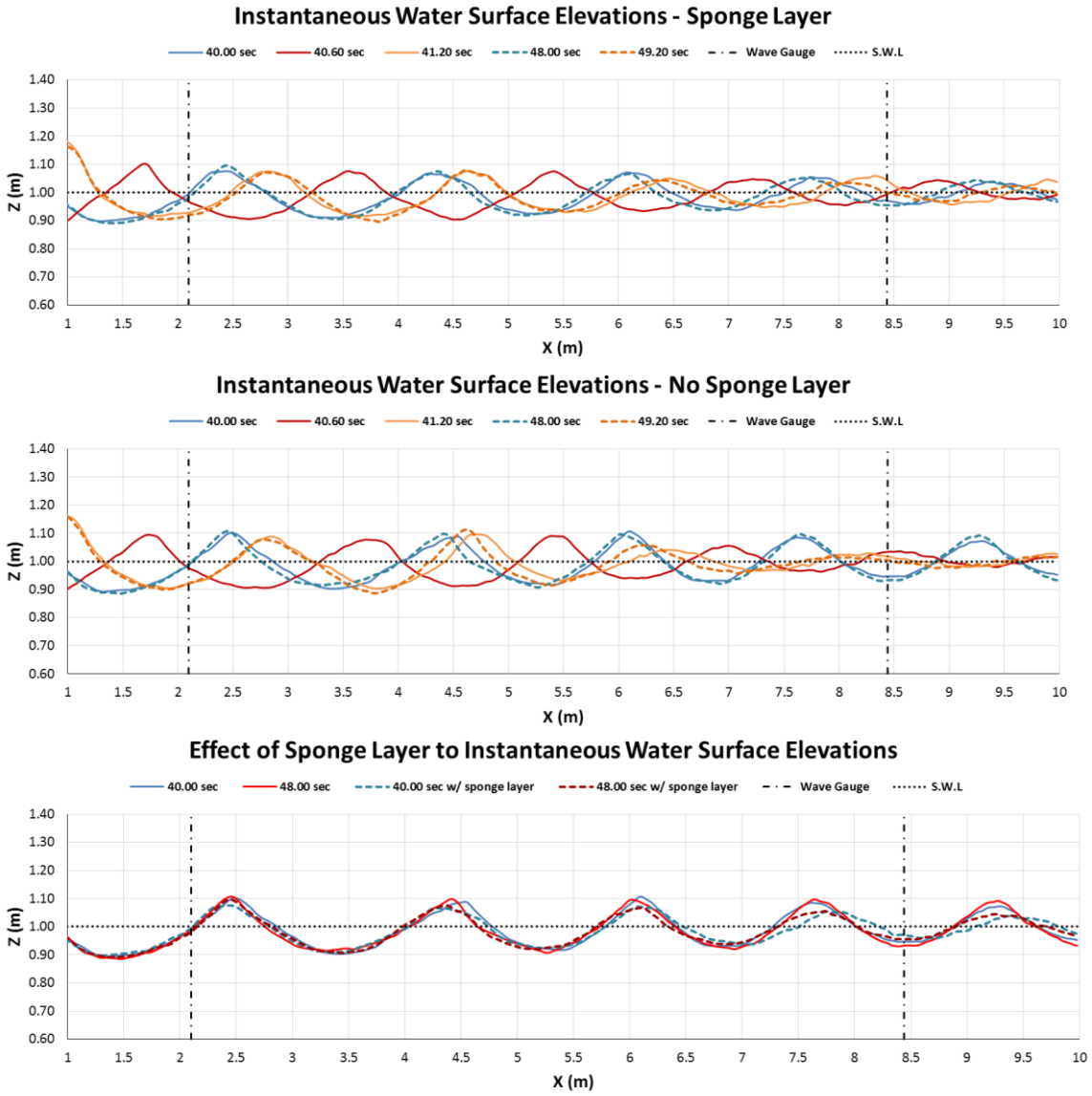

Figure 41: Instantaneous free surface profile of the wave maker case

From the Fig 41, we can see that the maxima have sharper angle than the minima, a feature that commonly appear on the nonlinear waves. The wavelength on both cases, calculated from peak to peak, is ranging between 1.70 m – 2.00 m. These values are around 9% - 28% larger than the estimated wavelength from the linear potential theory,

and even larger compared with the longest possible wavelength according to linear potential theory which is the deep water wavelength. The elongated wavelength of the simulated waves were also present in the solitary wave propagation studied by Vaughan (2005) and was connected to the choice of the artificial viscosity coefficient α. Finally, it can be deduced that the sponge layer has successfully absorbed the wave energy without changing others wave characteristics other than the wave height.

5. CONCLUSIONS

Both Smoothed Particle Hydrodynamics and Moving Particle Semi-implicit Method are mesh-free Lagrangian computational fluid dynamic methods that utilize weighted interpolation to solve the continuity and Navier-Stokes equation. Although having similar framework and interpolation method, SPH and MPS have several differences, especially on how the spatial derivatives are formulated, and how the pressure and the density are coupled. The SPH that is modeled using DualSPHysics program and the MPS that is modeled using an in-house program from Offshore System Simulation Lab Texas A&M University shows good agreements with experiment results, both quantitatively and quantitatively. From kinematics study of dam break case, it is found that the MPS has a higher sensitivity to viscosity value than the SPH and the kinematic viscosity value of $10^{-4} - 10^{-3}$ in the MPS model, is roughly equivalent to the dimensional artificial viscosity value $\alpha_0 c_0 h$ in the range of 0.027 – 0.23 in the SPH model. The SPH artificial viscosity coefficient value has a threshold of $\alpha \approx O(10^{-1})$ or $\frac{1}{8}\alpha_0 c_0 h \approx O(10^{-2})$, in which the kinematics will be started to be affected by the viscosity variation. Although DualSPHysics proved to be more superior than the MPS program in terms of computation time, the MPS can compensate by using less number of particles while maintaining the same accuracy as SPH with a larger number of particles.

Due to the discontinuity of velocity near the boundary, exaggerated pressure in the classical SPH with dynamic boundary condition is observed. The exaggerated pressure

caused an unphysical gap to emerge and make it impossible to measure the dynamic pressure using the wall particles pressure accurately. A direct relation between fluid particle's and wall particle's pressure such as observed in the Poisson equation of the MPS method are considered as promising solution. Adami boundary condition suits the need properly by calculating the wall particles pressure using the force balance relation between the fluid and wall particles. However, without the use of collision model, several fluid particles can still penetrate the wall particles, especially on the sharp corners. The use of the collision model only have a minor effect on the characteristic of the pressure profile and stability, thus can be combined with the Adami B.C. directly. The absence of the viscosity term in the Adami B.C. formulations, makes the boundary condition perform poorly when a high shear interaction between the wall and fluid particles are involved. Furthermore, the viscous interaction between the wall and the fluid particles need to be removed to avoid disturbance in the fluid flow's kinematics. A further study needs to be done to include the viscosity term and further improve the Adami B.C.

Piston type wave maker was simulated using SPH with the improved B.C, and the effectiveness of a sponge layer to absorb wave energy is studied. The sponge layer has successfully absorbed the incoming wave energy, without changing other wave characteristics. Viscous dissipation is observed to affect both the wave height and the wavelength of simulated wave. Further study on SPH viscosity formulation is needed to address the aforementioned problem properly.

REFERENCES

Altomare, C., Crespo, A. J. C., Rogers, B. D., Dominguez, J. M., Gironella, X., & Gómez-Gesteira, M. (2014). Numerical modelling of armour block sea breakwater with smoothed particle hydrodynamics. *Computers & Structures, 130*(0), 34-45.

Adami, S., Hu, X.Y., and Adams, N.A. (2012), "A Generalized Wall Boundary Condition for Smoothed Particle Hydrodynamics," *J. of Comp. Phys.*, 231, 7057-7075

Bakti, F.P., Kim, K.S., Kim, M.H., Park, J.C. (2015), "Comparative Study on Particle Method for Numerical Simulation," *Int. Soc. of Offshore and Polar Eng. Proc.* vol. 3, 424-431

Bonet, J. and Lok, T.-S.L. (1999), "Variational and Momentum Preservation Aspects of Smooth Particle Hydrodynamic Formulation," *Comput. Methods Appl. Mech. Engrg*, 180, 97-115

Crespo, A. J. C. (2008). "Application of the Smoothed Particle Hydrodynamics model SPHysics to free-surface hydrodynamics," *Ph.D. Thesis, Universidade De Vigo, Portugal*.

Crespo, A.J.C., Dominguez, J.M, Rogers, B.D, Gomez-Gesteira, M., Longshaw, S., Canelas, R., Vacondio, R., Barreiro, and A., Garcia-Feal, O. (2015), "DualSPHysics: Open-source Parallel CFD Solver Based on Smoothed Particle Hydrodynamics (SPH)", *Computer Physics Communications*, 187, 204-216

Dalrymple, R. A., and Rogers, B. D. (2006). "Numerical Modeling of Water Waves with the SPH Method." *Coast. Eng.*, 53, 141-147.

Dean, R. G., and Dalrymple, R. A. (1991). *Water Wave Mechanics for Engineers and Scientists*, Singapore ; Teaneck, NJ : World Scientific, c1991, .

Gingold, R.A. and Monaghan, J.J. (1977), "Smoothed Particle Hydrodynamics – Theory and Application to non Spherical Stars," *Mon. Not. of the R. Astron. Soc.*, 181, 375-389.

Gomez-Gesteira, M., Rogers, B. D., Crespo, A. J. C., Dalrymple, R. A., Narayanaswamy, M., & Dominguez, J. M. (2012a). SPHysics – development of a free-surface fluid solver – Part 1: Theory and formulations. *Computers & Geosciences, 48*(0), 289-299.

Gomez-Gesteira, M., Crespo, A. J. C., Rogers, B. D., Dalrymple, R. A., Dominguez, J. M., & Barreiro, A. (2012b). SPHysics – development of a free-surface fluid solver – Part 2: Efficiency and test cases. *Computers & Geosciences, 48*(0), 300-307.

Kim, K.S., Kim, M.H., and Park, J.C. (2014), "Development of Moving Particle Simulation Method for Multiliquid-Layer Sloshing," *Mathematical Problem in Engineering*

Koshizuka, S. and Oka, Y. (1996), "Moving-Particle Semi-implicit Method for Fragmentation of Incompressible Fluid,", *Nuclear Sci. and Engrg.*, 123, 421-434.

Lee, B.H., Park, J.C., and Kim, M.H. (2011), "Step-by-step Improvements of MPS Method in Simulating Violent Free-surface Motions and Impact Loads," *Comput. Methods Appl. Mech. Engrg.*, 200, 1113-1125.

Liu, G. R., and Liu, M. B. (2003). *Smoothed Particle Hydrodynamics : A Meshfree Particle Method,* Singapore ; London : World Scientific, 2003, .

Lo, E.Y.M and Shao, S. (2002), "Simulation of Near-Shore Solitary Wave Mechanics by an Incompressible SPH Method," *Applied Ocean Research,* 24, 275-286

Lucy, L.B. (1977), "A Numerical Approach to the Testing of the Fission Hypothesis," *Astron. J.*, 82, 1013-1024

Modave, A., Deleersnijder, É., Delhez, J.M. (2010). "On the parameters of absorbing layers for shallow water models," *Ocean Dynamic*., 60, 65–79.

Molteni, D., Grammauta, R., Vitanza, E. (2013). "Simple Absorbing Layer Conditions for Shallow Wave Simulations with Smoothed Particle Hydrodynamics." *Ocean Eng.*, 62(0), 78-90.

Monaghan, J. J. (1989). "On the problem of penetration in particle methods," *Journal of Computational Physics, 82*(1), 1-15

Monaghan, J.J. (1992), "Smoothed Particle Hydrodynamic," *Annu. Rev. Astron. Appl.*, 30, 543-574

Monaghan, J.J. (1994), "Simulating Free Surface Flows with SPH," *J. of Comp. Phys.*, 110, 399-406

Monaghan, J. J. (2000). "SPH without a Tensile Instability." *Journal of Computational Physics,* 159(2), 290-311.

Monaghan, J.J. (2012), "Smoothed Particle Hydrodynamics and Its Diverse Applications," *Annu. Rev. Fluid Mech.,* 44, 323-346

Morris, J.P., Fox, P.J., and Zhu, Yi (1997), "Modeling Low Reynolds Number Incompressible Flows Using SPH," *J. of Comp. Phys.*, 136, 214-226

Pelfrene, J. (2011). "Study of the SPH method for simulation of regular and breaking waves," *M.Eng. Thesis, Universiteit Gent, Belgium*.

Price, J. F. (2006). "Lagrangian and Eulerian Representations of Fluid Flow: Kinematics and the Equations of Motion," *Lecture Note, Woods Hole Oceanographic Institution*.

Randles, P. W., & Libersky, L. D. (1996). "Smoothed Particle Hydrodynamics: Some recent improvements and applications," *Computer Methods in Applied Mechanics and Engineering, 139*(1–4), 375-408.

Rogers, B. D., Dalrymple, R. A., & Stansby, P. K. (2010). "Simulation of caisson breakwater movement using 2-D SPH," *Journal of Hydraulic Research, 48*, 135-141.

Schwaiger, H. F. (2008). "An implicit corrected SPH formulation for thermal diffusion with linear free surface boundary conditions". *International Journal for Numerical Methods in Engineering, 75*(6), 647-671.

Shakibaeinia, A. and Jin, Y.C. (2011) "A MPS Based Mesh-free Particle Method for Modeling Open Channel Flows" *J. of Hydraulic Engrg*, ASCE, 137(11): 1375-1384.

Tanaka, M. and Masunaga, T. (2010), "Stabilization and Smoothing of Pressure in MPS Method by Quasi-Compressibility," *J. of Compt. Phys.*, 229, 4279-4290

Ulrich, C., Leonardi, M., & Rung, T. (2013). "Multi-physics SPH simulation of complex marine-engineering hydrodynamic problems," *Ocean Engineering, 64*(0), 109-121.

Vaughan, G. L. (2005). "Simulating breaking waves using smoothed particle hydrodynamics," *Ph.D. Thesis, University of Waikato, Hamilton, New Zealand*.

Verlet, L. (1967). "Computer Experiments on Classical Fluids. I. Thermodynamical Properties of Lennard-Jones Molecules," *Phys. Rev.*, 159, 98-103.

APPENDIX A

Default SPHysics Algorithm

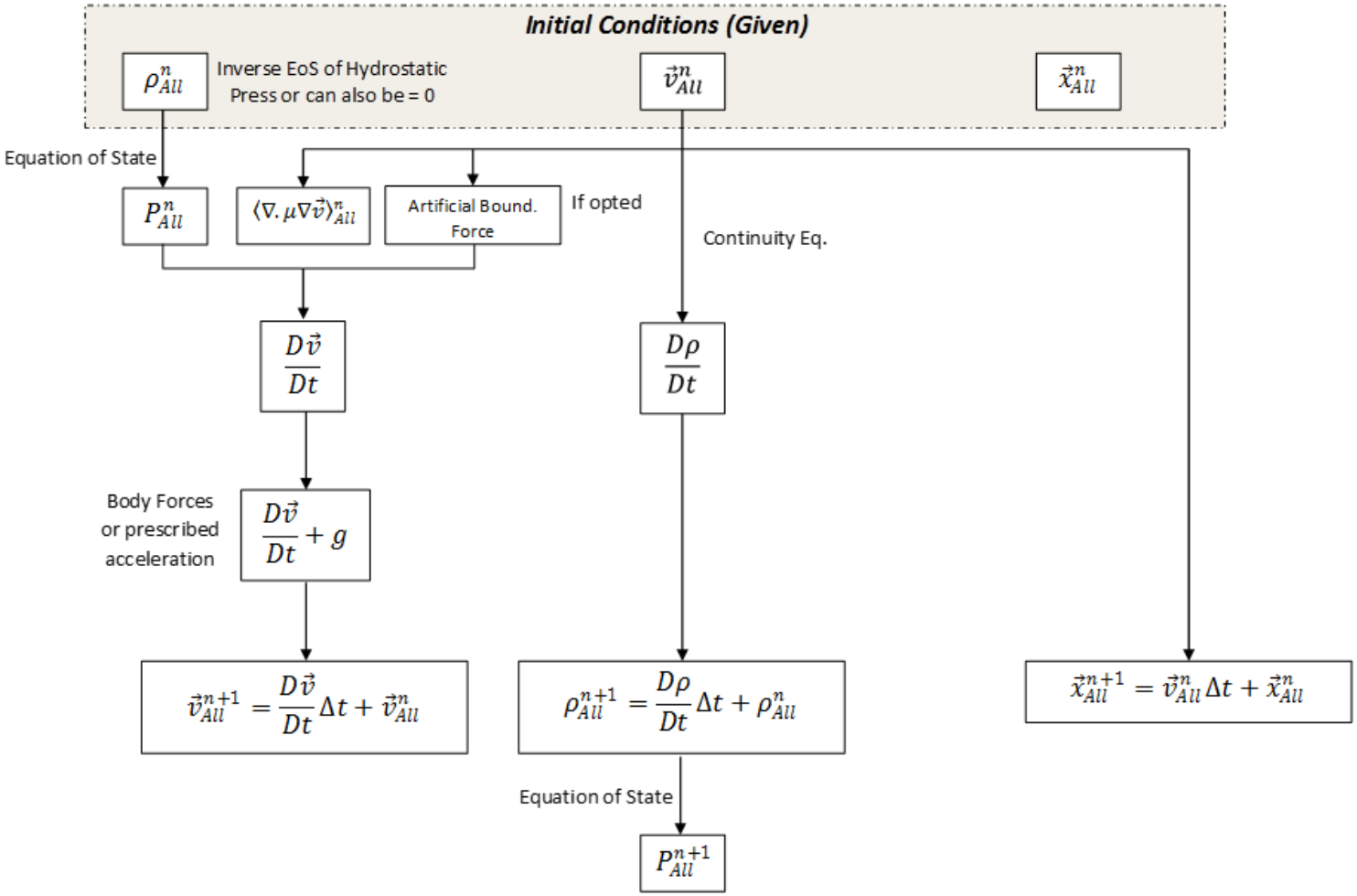

APPENDIX B

Modified SPHysics Algorithm with Adami B.C. and Collision Model